Coarray Tensor Direction-of-Arrival Estimation

Hang Zheng , *Graduate Student Member, IEEE*, Chengwei Zhou , *Member, IEEE*,
Zhiguo Shi , *Senior Member, IEEE*, Yujie Gu , *Senior Member, IEEE*, and Yimin D. Zhang , *Fellow, IEEE*

Abstract—Augmented coarrays can be derived from spatially undersampled signals of sparse arrays for underdetermined direction-of-arrival (DOA) estimation. With the extended dimension of sparse arrays, the sampled signals can be modeled as sub-Nyquist tensors, thereby enabling coarray tensor processing to enhance the estimation performance. The existing methods, however, are not applicable to generalized multi-dimensional sparse arrays, such as sparse planar array and sparse cubic array, and have not fully exploited the achievable source identifiability. In this paper, we propose a coarray tensor DOA estimation algorithm for multi-dimensional structured sparse arrays and investigate an optimal coarray tensor structure for source identifiability enhancement. Specifically, the cross-correlation tensor between sub-Nyquist tensor signals is calculated to derive a coarray tensor. Based on the uniqueness condition for coarray tensor decomposition, the achievable source identifiability is analysed. Furthermore, to enhance the source identifiability, a dimension increment approach is proposed to embed shifting information in the coarray tensor. The shifting-embedded coarray tensor is subsequently reshaped to optimize the source identifiability. The resulting maximum number of degrees-of-freedom is theoretically proved to exceed the number of physical sensors. Hence, the optimally reshaped coarray tensor can be decomposed for underdetermined DOA estimation with closed-form solutions. Simulation results demonstrate the effectiveness of the proposed algorithm in both underdetermined and overdetermined cases.

Index Terms—Coarray tensor, direction-of-arrival estimation, source identifiability, sparse array, sub-Nyquist tensor.

Hang Zheng is with the College of Information Science and Electronic Engineering, Zhejiang University, Hangzhou 310027, China (e-mail: hangzheng@zju.edu.cn).

Chengwei Zhou is with the College of Information Science and Electronic Engineering, Zhejiang University, Hangzhou 310027, China, and also with the Key Laboratory of Collaborative Sensing and Autonomous Unmanned Systems of Zhejiang Province, Hangzhou 310015, China (e-mail: zhouchw@zju.edu.cn).

Zhiguo Shi is with the College of Information Science and Electronic Engineering, Zhejiang University, Hangzhou 310027, China, and also with the International Joint Innovation Center, Zhejiang University, Haining 314400, China (e-mail: shizg@zju.edu.cn).

Yujie Gu is with the Advanced Safety & User Experience, Aptiv, Agoura Hills, CA 91301 USA (e-mail: guyujie@hotmail.com).

Yimin D. Zhang is with the Department of Electrical and Computer Engineering, Temple University, Philadelphia, PA 19122 USA (e-mail: ydzhang@temple.edu).

Digital Object Identifier 10.1109/TSP.2023.3260559

I. INTRODUCTION

DIRECTION-OF-ARRIVAL (DOA) estimation using sensor arrays plays an important role in many applications including radar, sonar, and wireless communication [2], [3]. However, traditional uniform arrays have to receive signals at the Nyquist sampling rate. As such, the system complexity often becomes infeasible or impractical as the size of array increases. To break through the limit of Nyquist sampling theorem, sparse arrays have recently drawn tremendous attention due to their ability to receive signals at a sub-Nyquist sampling rate [4], [5], [6], [7]. A series of efforts have been made to achieve DOA estimation for sparse arrays, which can alleviate the system burden using sub-Nyquist signals while offering an enlarged array aperture [8], [9], [10], [11], [12].

Among these sparse arrays being developed, the coprime array [4] and nested array [5] with systematic structures are popularly considered. DOA estimation methods exploiting these structured sparse arrays are then developed [13], [14], [15]. In particular, an array decomposition method is proposed for the coprime linear array [16], where the Multiple Signal Classification (MUSIC) is separately performed on the coprime subarray signals, and their closest spectral peaks are searched for ambiguity-free DOA estimation. However, the array decomposition method causes at least half degrees-of-freedom (DOFs) loss and, as a result, fails to deal with underdetermined cases. To increase the number of DOFs, augmented virtual arrays are derived from the second-order sub-Nyquist signal statistics, such that the coarray MUSIC can be implemented to achieve underdetermined DOA estimation [13], [17]. After that, the coarray Estimation of Signal Parameters via Rotational Invariance Technique (ESPRIT) method [18], the coarray matrix completion method [19], [20], and the coarray matrix reconstruction method [21], [22], [23] have been proposed within the framework of coarray processing.

While most of the existing methods deal with one-dimensional (1-D) arrays which only sense angular information in azimuth, real-world applications often require multi-dimensional information, such as in both azimuth and elevation [24]. As such, the arrays need to be extended to two-dimensional (2-D) [25] and even three-dimensional (3-D) configurations [26]. In these cases, the above-mentioned methods still follow the principle of matrix-based signal processing, where the multi-dimensional sub-Nyquist signals with multiple snapshots are simply flattened into a matrix, and the coarray

signal is derived from vectorizing the second-order covariance matrix. As a result, the structural characteristics of the sub-Nyquist signals cannot be exploited, resulting in a performance deterioration. Motivated by this fact, in this paper, we investigate a more effective strategy of multi-dimensional sub-Nyquist signal processing to achieve DOA estimation.

Tensor, as an extension of matrix, has been adopted to model multi-dimensional signals in array processing applications. Meanwhile, the underlying characteristics of tensor signals can be exploited via tensor decompositions [27], among which canonical polyadic decomposition (CPD) [28] is the representative one. In [29], tensor decomposition is applied to multi-dimensional uniform array signals for DOA estimation. By incorporating an array virtual translation technique, a Vandermonde-constrained tensor decomposition-based subspace method is proposed to enhance the estimation accuracy [30]. Furthermore, tensor DOA estimation has been intensively implemented under deployments of electromagnetic vector sensor [31], massive antenna array [32], and multiple-input-multiple-output (MIMO) radar [33]. Meanwhile, a tensor reconstruction approach is designed for coherent sources estimation with uniform arrays [34]. However, the above-mentioned methods conform to the Nyquist sampling theorem, and the resulting DOA estimation performance is still restricted by the uniform array aperture.

More recently, sub-Nyquist tensor processing for DOA estimation has been proposed to seek the performance breakthrough [35]. In particular, the sub-Nyquist *temporal* sampling is investigated in [36], [37], where temporally undersampled tensor signals are completed for DOA estimation. However, they do not consider the sub-Nyquist spatial sampling using sparse arrays. Although the sub-Nyquist radar deploys thinned arrays for sub-Nyquist *spatial* sampling [38], the sub-Nyquist tensor is directly recovered for DOA estimation, whereas the second-order coarray tensor statistics are not derived. By pushing coarray processing to the tensorial domain, a tensor MUSIC method is proposed for nested vector-sensor arrays using the coarray statistics [35]. Furthermore, diverse coarray tensor processing approaches have been proposed such as the coupled coarray tensor CPD [39] and the complex parallel factor analysis (COMFAC) for nested MIMO radar [40]. Nevertheless, these methods only consider the sparse L-shaped array or collocated linear array geometries, whose corresponding coarray tensor derivation is not applicable to generalized multi-dimensional sparse arrays, especially the sparse planar arrays or sparse cubic arrays. Regarding this, a self-correlation tensor processing method is proposed for co-prime planar array to improve the DOA estimation accuracy and increase the number of DOFs [41]. Unfortunately, none of the above-mentioned methods have explored the optimal source identifiability. Although the identifiability for parameter estimation is improved by respectively exploiting MIMO waveform diversity [42] and tensor decomposability [43], the principle of identifiability enhancement for the coarray tensor has not been investigated. Hence, it remains an open problem to excavate the potential of the coarray tensor to achieve DOA estimation with an optimal source identifiability.

In this paper, we propose a novel coarray tensor DOA estimation algorithm for multi-dimensional structured sparse arrays. The array received signals are represented by a pair of sub-Nyquist tensors, based on which the cross-correlation tensor statistics are calculated. Then, we derive a cross-correlation-based augmented virtual array, whose equivalent signal is modeled as a coarray tensor. The relationship between the coarray tensor structure and the source identifiability is established, based on which a dimension increment approach is proposed to embed shifting information in the coarray tensor to enhance the source identifiability. Subsequently, directionally reshaping and spatially reshaping approaches are designed for the shifting-embedded coarray tensor to refine its structure. In particular, by formulating corresponding coarray tensor segmentation window optimization problems and comparing the resulting number of DOFs, the optimally reshaped coarray tensor with the best source identifiability is devised. As such, coarray tensor decomposition leads to closed-form solutions of the azimuth and elevation, which works for both underdetermined and overdetermined cases. Simulation results verify the superior performance of the proposed algorithm compared to existing matrix-based and tensor-based methods.

The concept of completing missing slices in the coarray tensor corresponding to partially augmentable sparse array is considered in [44], where the missing slices are sufficiently dispersed to ensure the best coarray tensor completion performance. The main contribution of this paper, on the other hand, lies in the optimization of source identifiability for coarray tensor processing with generalized sparse array configurations. Such results are novel and have not been considered in [44]. In [26], we devise a cross-correlation tensor-based subspace method for sparse cubic array DOA estimation with a high estimation accuracy, whereas both computational efficiency and source identifiability are degraded. In [45], we develop a sub-Nyquist tensor train decomposition method to enhance the computational efficiency of DOA estimation with sparse cubic array, whereas the source identifiability is still sacrificed. In this paper, we particularly investigate the optimal source identifiability for generalized multi-dimensional structured sparse arrays to achieve coarray tensor-based underdetermined DOA estimation. Some preliminary results of this work are presented in the conference paper [1]. In this paper, we further establish a clear relationship between the coarray tensor structure and the achievable source identifiability. Based on that, two coarray tensor reshaping approaches are developed to realize the optimal source identifiability. In addition, we provide details of source identifiability optimization problems, and theoretically analyse the maximum number of DOFs.

The rest of this paper is organized as follows. In Section II, we introduce preliminaries about notations and tensor operations. In Section III, we present the sub-Nyquist tensor signal model, and in Section IV, we formulate the corresponding coarray tensor. Then, in Section V, we propose an optimal source identifiability enhancement strategy to achieve underdetermined DOA estimation. We demonstrate simulation results in Section VI, and draw our conclusion in Section VII.

II. PRELIMINARIES

In this section, we provide necessary preliminaries about notations and tensor operations including CPD and generalized tensor reshaping of a canonical polyadic (CP) model.

Notations: Scalars, vectors, matrices, and tensors are respectively denoted by lower-case letters, lower-case bold-face letters, upper-case bold-face letters, and calligraphic bold-face letters, e.g., a, $\boldsymbol{a}$, $\boldsymbol{A}$, and $\boldsymbol{\mathcal{A}}$. $\times_i$ denotes the mode-i tensor-matrix product. $\boldsymbol{\mathcal{A}}_1 \overset{i_2}{\underset{i_1}{\times}} \boldsymbol{\mathcal{A}}_2$ denotes the tensor contraction along the i_1-th dimension of $\boldsymbol{\mathcal{A}}_1$ and the i_2-th dimension of $\boldsymbol{\mathcal{A}}_2$. $(\cdot)^{\mathrm{T}}$, $(\cdot)^{\mathrm{H}}$, $(\cdot)^*$, and $(\cdot)^{\dagger}$ denote the transpose, the Hermitian transpose, the conjugation, and the pseudoinverse operators, respectively. The notation $\mathrm{E}\{\cdot\}$ represents the statistical expectation. $\llbracket \cdot \rrbracket$ denotes the CPD representation of a tensor, while $\kappa(\cdot)$ denotes the Kruskal's rank. The outer product, Kronecker product, and the Khatri-Rao product are denoted by $\circ$, $\otimes$, and $\odot$, respectively. $[\cdot]_i$ denotes the mode-i unfolding of a tensor, and $[\cdot]_{\sqcup_i}$ denotes the tensor concatenation along the i-th dimension. $\|\cdot\|_{\mathrm{F}}$ denotes the Frobenius norm. $\min(\cdot)$, $\max(\cdot)$, and $\mathrm{mod}(\cdot)$ denote the minimum, maximum, and modulo operators, respectively. $\angle$ represents the phase of a complex number. $|\cdot|$ represents the cardinality of a set. $\jmath = \sqrt{-1}$ denotes the imaginary unit. The identity matrix and all-zero matrix with appropriate dimensions are respectively denoted by $\boldsymbol{I}$ and $\boldsymbol{0}$, whereas the identity tensor is denoted by $\boldsymbol{\mathcal{I}}$. Finally, the set of complex numbers is denoted by $\mathbb{C}$.

CPD: The CPD factorizes an N-dimensional tensor $\boldsymbol{\mathcal{A}} \in \mathbb{C}^{I_1 \times I_2 \times \cdots \times I_N}$ into the sum of R outer products, i.e.,

$$\boldsymbol{\mathcal{A}} = \sum_{r=1}^{R} \eta_r \boldsymbol{a}_1(r) \circ \boldsymbol{a}_2(r) \circ \cdots \circ \boldsymbol{a}_N(r)$$
$$\triangleq \llbracket \boldsymbol{\eta}; \boldsymbol{A}_1, \boldsymbol{A}_2, \ldots, \boldsymbol{A}_N \rrbracket, \quad (1)$$

where $\boldsymbol{a}_n(r) \in \mathbb{C}^{I_n}$ is the CP factor with $\boldsymbol{A}_n = [\boldsymbol{a}_n(1), \boldsymbol{a}_n(2), \ldots, \boldsymbol{a}_n(R)] \in \mathbb{C}^{I_n \times R}$ being the corresponding factor matrix, $n = 1, 2, \ldots, N$, and $\boldsymbol{\eta} = [\eta_1, \eta_2, \ldots, \eta_R]^{\mathrm{T}}$ is the scaling coefficient vector. The CPD of $\boldsymbol{\mathcal{A}}$ is unique as long as it satisfies the following Kruskal's condition[1]

$$\kappa(\boldsymbol{A}_1) + \kappa(\boldsymbol{A}_2) + \cdots + \kappa(\boldsymbol{A}_N) \geqslant 2R + (N-1). \quad (2)$$

Generalized Tensor Reshaping of CP Model: Let dimension sets $\{\mathbb{S}_j, j = 1, 2, \ldots, J\}$ be a partition of $\{1, 2, \ldots, N\}$, then the N-dimensional tensor $\boldsymbol{\mathcal{A}}$ in (1) can be reshaped to a $\prod_{n_1 \in \mathbb{S}_1} I_{n_1} \times \prod_{n_2 \in \mathbb{S}_2} I_{n_2} \times \cdots \times \prod_{n_J \in \mathbb{S}_J} I_{n_J}$ J-dimensional tensor

$$\langle \boldsymbol{\mathcal{A}} \rangle_{\mathbb{S}_1, \mathbb{S}_2, \ldots, \mathbb{S}_J} = \sum_{r=1}^{R} \eta_r \bar{\boldsymbol{a}}_1(r) \circ \bar{\boldsymbol{a}}_2(r) \circ \cdots \circ \bar{\boldsymbol{a}}_J(r). \quad (3)$$

---

[1]When one of the factor matrices has a full column rank, a necessary and sufficient condition for uniqueness of CPD is established [43]. This condition, however, is restrictive. Under deployment of generalized sparse arrays, (2) is imposed as a general and sufficient condition, which is commonly used in the literature relevant to tensor-based DOA estimation [40], [46].
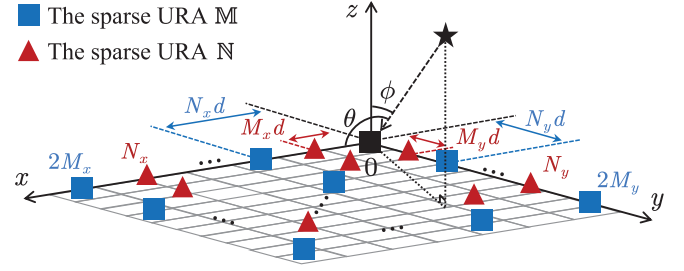

Fig. 1. The geometry of the coprime planar array.

The reshaped tensor still conforms to the CP model, where $\bar{\boldsymbol{a}}_j(r) = \prod_{n_j \in \mathbb{S}_j} \otimes \boldsymbol{a}_{n_j}(r) \in \mathbb{C}^{\prod_{n_j \in \mathbb{S}_j} I_{n_j}}$ is the CP factor, $j = 1, 2, \ldots, J$.

III. SUB-NYQUIST TENSOR SIGNAL MODEL

Among various types of sparse arrays, we adopt the coprime array [4] as an example, but the results can be extended to a general class of multi-dimensional sparse arrays including nested array, coprime array and their variants [47]. As shown in Fig. 1, a coprime planar array $\mathbb{P}$ consists of a pair of sparse uniform rectangular arrays (URAs) $\mathbb{M}$ and $\mathbb{N}$. There are $2M_x \times 2M_y$ sensors in $\mathbb{M}$ and $N_x \times N_y$ sensors in $\mathbb{N}$, where $\{M_x, N_x\}$ and $\{M_y, N_y\}$ are respective pairs of coprime integers. The inter-element spacings for the sparse URA $\mathbb{M}$ are $N_x d$ and $N_y d$ along the x-axis and the y-axis, respectively. Here, d equals to half of the source signal wavelength. Similarly, the inter-element spacings for the sparse URA $\mathbb{N}$ are $M_x d$ and $M_y d$ along the x-axis and the y-axis, respectively. Due to the coprime deployment between the two sparse URAs, their sensors do not overlap except for the one at the origin of the coordinate system $(0, 0, 0)$. Therefore, the total number of sensors in the coprime planar array $\mathbb{P}$ is $|\mathbb{P}| = 4M_x M_y + N_x N_y - 1$.

Assume that K uncorrelated far-field narrowband source signals impinge on the coprime planar array $\mathbb{P}$, where $\theta_k \in [-\pi/2, \pi/2]$ and $\phi_k \in [0, \pi]$ are respectively the azimuth and elevation of the k-th source, $k = 1, 2, \ldots, K$. Traditionally, the matrix-based model will represent the sparse URA received signals at each time slot by a vector $\boldsymbol{x}(t) = [\boldsymbol{x}_{\mathbb{M}}^{\mathrm{T}}(t), \boldsymbol{x}_{\mathbb{N}}^{\mathrm{T}}(t)]^{\mathrm{T}} \in \mathbb{C}^{4M_x M_y + N_x N_y}$, where

$$\boldsymbol{x}_{\mathbb{M}}(t) = \sum_{k=1}^{K} s_k(t) \boldsymbol{a}_{\mathbb{M}}(\mu_k) \otimes \boldsymbol{a}_{\mathbb{M}}(\nu_k) + \boldsymbol{n}_{\mathbb{M}}(t) \in \mathbb{C}^{4M_x M_y},$$

$$\boldsymbol{x}_{\mathbb{N}}(t) = \sum_{k=1}^{K} s_k(t) \boldsymbol{a}_{\mathbb{N}}(\mu_k) \otimes \boldsymbol{a}_{\mathbb{N}}(\nu_k) + \boldsymbol{n}_{\mathbb{N}}(t) \in \mathbb{C}^{N_x N_y}. \quad (4)$$

Here,

$$\boldsymbol{a}_{\mathbb{M}}(\mu_k) = \left[1, e^{-\jmath \pi N_x \mu_k}, \ldots, e^{-\jmath \pi N_x (2M_x - 1)\mu_k}\right]^{\mathrm{T}},$$

$$\boldsymbol{a}_{\mathbb{M}}(\nu_k) = \left[1, e^{-\jmath \pi N_y \nu_k}, \ldots, e^{-\jmath \pi N_y (2M_y - 1)\nu_k}\right]^{\mathrm{T}} \quad (5)$$

are respectively the steering vectors of $\mathbb{M}$ along the x-axis and the y-axis with directional parameters

$$\mu_k = \sin \phi_k \cos \theta_k,$$
$$\nu_k = \sin \phi_k \sin \theta_k, \tag{6}$$

and

$$\boldsymbol{a}_{\mathbb{N}}(\mu_k) = \left[1, e^{-\jmath \pi M_x \mu_k}, \ldots, e^{-\jmath \pi M_x (N_x-1)\mu_k} \right]^{\mathrm{T}},$$

$$\boldsymbol{a}_{\mathbb{N}}(\nu_k) = \left[1, e^{-\jmath \pi M_y \nu_k}, \ldots, e^{-\jmath \pi M_y (N_y-1)\nu_k} \right]^{\mathrm{T}} \tag{7}$$

are respectively the steering vectors of $\mathbb{N}$ along the x-axis and the y-axis, $s_k(t)$ is the source signal at the t-th time slot, $t = 1, 2, \ldots, T$, $\boldsymbol{n}_{\mathbb{M}}(t), \boldsymbol{n}_{\mathbb{N}}(t) \sim \mathcal{CN}(\boldsymbol{0}, \sigma_n^2 \boldsymbol{I})$ are independent and identically distributed (i.i.d.) additive white Gaussian noise vectors with σ_n^2 being the noise power. Then, the T snapshots of the two sparse URAs are stacked together to form a sub-Nyquist signal matrix $\boldsymbol{X} = [\boldsymbol{x}(1), \boldsymbol{x}(2), \ldots, \boldsymbol{x}(T)] \in \mathbb{C}^{(4M_x M_y + N_x N_y) \times T}$, whose auto-correlation $\mathrm{E}\{\boldsymbol{x}(t)\boldsymbol{x}^{\mathrm{H}}(t)\}$ is calculated for deriving the second-order coarray statistics. However, the above matrix-based signal model ignores the original 3-D spatio-temporal structure of the sub-Nyquist signals, resulting in an inevitable performance deterioration.

To avoid the structural information loss, we model the sparse URA signals at the t-th time slot by two independent matrices

$$\boldsymbol{X}_{\mathbb{M}}(t) = \sum_{k=1}^{K} s_k(t) \boldsymbol{a}_{\mathbb{M}}(\mu_k) \circ \boldsymbol{a}_{\mathbb{M}}(\nu_k) + \boldsymbol{N}_{\mathbb{M}}(t) \in \mathbb{C}^{2M_x \times 2M_y},$$

$$\boldsymbol{X}_{\mathbb{N}}(t) = \sum_{k=1}^{K} s_k(t) \boldsymbol{a}_{\mathbb{N}}(\mu_k) \circ \boldsymbol{a}_{\mathbb{N}}(\nu_k) + \boldsymbol{N}_{\mathbb{N}}(t) \in \mathbb{C}^{N_x \times N_y}, \tag{8}$$

where $\boldsymbol{N}_{\mathbb{M}}(t), \boldsymbol{N}_{\mathbb{N}}(t) \sim \mathcal{CN}(\boldsymbol{0}, \sigma_n^2 \boldsymbol{\mathcal{I}})$ are i.i.d. additive white Gaussian noise matrices. After that, the total T snapshots of $\boldsymbol{X}_{\mathbb{M}}(t)$ and $\boldsymbol{X}_{\mathbb{N}}(t)$ are respectively concatenated along an additional temporal dimension to generate two 3-D sub-Nyquist tensors

$$\boldsymbol{\mathcal{X}}_{\mathbb{M}} = [\boldsymbol{X}_{\mathbb{M}}(1), \boldsymbol{X}_{\mathbb{M}}(2), \ldots, \boldsymbol{X}_{\mathbb{M}}(T)]_{\sqcup_3} \in \mathbb{C}^{2M_x \times 2M_y \times T}$$

$$= \sum_{k=1}^{K} \boldsymbol{a}_{\mathbb{M}}(\mu_k) \circ \boldsymbol{a}_{\mathbb{M}}(\nu_k) \circ \boldsymbol{s}_k + \boldsymbol{\mathcal{N}}_{\mathbb{M}}, \tag{9}$$

$$\boldsymbol{\mathcal{X}}_{\mathbb{N}} = [\boldsymbol{X}_{\mathbb{N}}(1), \boldsymbol{X}_{\mathbb{N}}(2), \ldots, \boldsymbol{X}_{\mathbb{N}}(T)]_{\sqcup_3} \in \mathbb{C}^{N_x \times N_y \times T}$$

$$= \sum_{k=1}^{K} \boldsymbol{a}_{\mathbb{N}}(\mu_k) \circ \boldsymbol{a}_{\mathbb{N}}(\nu_k) \circ \boldsymbol{s}_k + \boldsymbol{\mathcal{N}}_{\mathbb{N}}, \tag{10}$$

where $\boldsymbol{s}_k = [s_k(1), s_k(2), \ldots, s_k(T)]^{\mathrm{T}}$ is the signal waveform vector, and $\boldsymbol{\mathcal{N}}_{\mathbb{M}}, \boldsymbol{\mathcal{N}}_{\mathbb{N}}$ are the noise tensors. Note that, the signal parts in $\boldsymbol{\mathcal{X}}_{\mathbb{M}}$ (9) and $\boldsymbol{\mathcal{X}}_{\mathbb{N}}$ (10) conform to the CP model as illustrated in (1).

Unlike the traditional matrix-based signal model, the formulated sub-Nyquist tensors $\boldsymbol{\mathcal{X}}_{\mathbb{M}}$ and $\boldsymbol{\mathcal{X}}_{\mathbb{N}}$ cannot be simply stacked to form a single tensor due to their different dimensions. Therefore, the conventional auto-correlation operation is not applicable to the sub-Nyquist tensors for calculating their second-order tensor statistics. In this regard, the cross-correlation between the sub-Nyquist tensors is proposed, and the four-dimensional (4-D) cross-correlation tensor $\boldsymbol{\mathcal{R}} \in \mathbb{C}^{2M_x \times 2M_y \times N_x \times N_y}$ can be calculated as

$$\boldsymbol{\mathcal{R}} = \mathrm{E}\left\{ \boldsymbol{X}_{\mathbb{M}}(t) \circ \boldsymbol{X}_{\mathbb{N}}^*(t) \right\}$$

$$= \sum_{k=1}^{K} \sigma_k^2 \boldsymbol{a}_{\mathbb{M}}(\mu_k) \circ \boldsymbol{a}_{\mathbb{M}}(\nu_k) \circ \boldsymbol{a}_{\mathbb{N}}^*(\mu_k) \circ \boldsymbol{a}_{\mathbb{N}}^*(\nu_k) + \boldsymbol{\mathcal{N}},$$

$$\tag{11}$$

where $\sigma_k^2 = \mathrm{E}\{s_k(t)s_k^*(t)\}$ represents the power of the k-th source, and $\boldsymbol{\mathcal{N}} = \mathrm{E}\{\boldsymbol{N}_{\mathbb{M}}(t) \circ \boldsymbol{N}_{\mathbb{N}}^*(t)\}$ is the noise term with only the $(1, 1, 1, 1)$-th element being σ_n^2 while all others are 0. In practice, the cross-correlation tensor $\boldsymbol{\mathcal{R}}$ can be estimated as

$$\hat{\boldsymbol{\mathcal{R}}} = \frac{1}{T} \boldsymbol{\mathcal{X}}_{\mathbb{M}} \underset{3}{\overset{3}{\times}} \boldsymbol{\mathcal{X}}_{\mathbb{N}}^*, \tag{12}$$

which averages the tensor contraction between the two sub-Nyquist tensors along the temporal dimension.

IV. COARRAY TENSOR DERIVATION

In this section, we derive an augmented virtual uniform array, and model its equivalent signal as a coarray tensor. We analyse the uniqueness condition for coarray tensor decomposition, and then propose a dimension increment approach for the coarray tensor to enhance the source identifiability.

A. Virtual Uniform Cuboid Array Formulation

For structured sparse arrays, augmented virtual arrays can be derived from the second-order sub-Nyquist signal statistics. The equivalent second-order signal of the derived virtual array (i.e., coarray signal) can then be processed to achieve Nyquist-matched DOA estimation. To this end, we derive a virtual array from the cross-correlation tensor $\boldsymbol{\mathcal{R}}$ (11) corresponding to the coprime planar array $\mathbb{P}$. Specifically, the CP factor pairs $\{\boldsymbol{a}_{\mathbb{M}}(\mu_k), \boldsymbol{a}_{\mathbb{N}}^*(\mu_k)\}$ and $\{\boldsymbol{a}_{\mathbb{M}}(\nu_k), \boldsymbol{a}_{\mathbb{N}}^*(\nu_k)\}$ of $\boldsymbol{\mathcal{R}}$ are capable of generating difference sets

$$\mathbb{D}_x = \{m_x N_x - n_x M_x | m_x = 0, 1, \cdots, 2M_x - 1,$$
$$n_x = 0, 1, \cdots, N_x - 1\},$$
$$\mathbb{D}_y = \{m_y N_y - n_y M_y | m_y = 0, 1, \cdots, 2M_y - 1,$$
$$n_y = 0, 1, \cdots, N_y - 1\}, \tag{13}$$

which yield a discontinuous virtual planar array $\mathbb{D} = \{(x_{\mathbb{D}}, y_{\mathbb{D}}) | x_{\mathbb{D}} = \mathbb{D}_x d, y_{\mathbb{D}} = \mathbb{D}_y d\}$, as shown in Fig. 2(a). Hence, we combine the first and third dimensions $\{1, 3\}$, as well as the second and fourth dimensions $\{2, 4\}$ of $\boldsymbol{\mathcal{R}}$ to generate Kronecker products of the CP factor pairs. According to the definition of
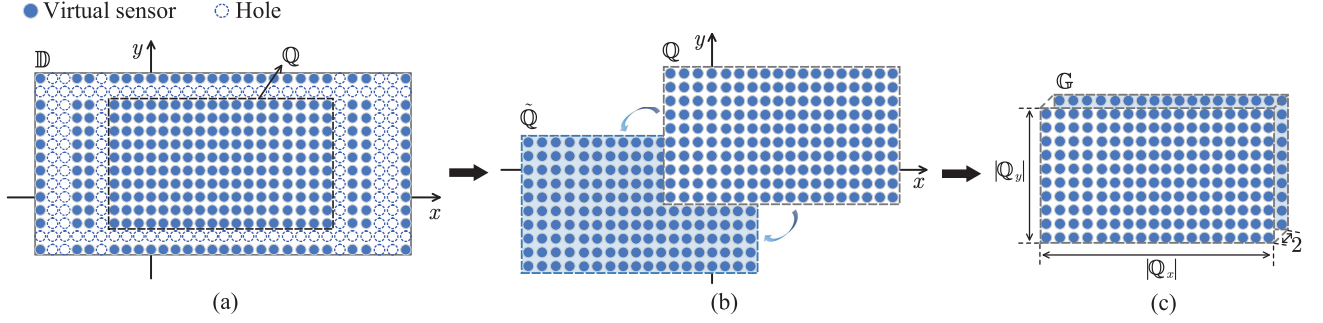
Fig. 2. Illustration of the virtual array geometries. (a) The discontinuous virtual planar array $\mathbb{D}$ and its constituting virtual URA $\mathbb{Q}$. (b) The mirrored extension $\tilde{\mathbb{Q}}$ of the virtual URA $\mathbb{Q}$. (c) The virtual UCA $\mathbb{G}$.

generalized tensor reshaping in (3), $\mathcal{R}$ can be reshaped as

$$\boldsymbol{R} \triangleq \langle \mathcal{R} \rangle_{\{1,3\},\{2,4\}} \in \mathbb{C}^{2M_xN_x \times 2M_yN_y}$$

$$= \sum_{k=1}^{K} \sigma_k^2 \left[\boldsymbol{a}_{\mathbb{N}}^*(\mu_k) \otimes \boldsymbol{a}_{\mathbb{M}}(\mu_k) \right] \circ \left[\boldsymbol{a}_{\mathbb{N}}^*(\nu_k) \otimes \boldsymbol{a}_{\mathbb{M}}(\nu_k) \right] + \boldsymbol{N},$$

(14)

where $\boldsymbol{N}$ is the reshaped noise term with only the $(1,1)$-th element being σ_n^2 while all others are 0.

It is noted that the difference sets $\mathbb{D}_x$ and $\mathbb{D}_y$ in (13) contain the following contiguous subsets [47]

$$\mathbb{Q}_x = \{-N_x+1, -N_x+2, \ldots, M_xN_x+M_x-1\},$$

$$\mathbb{Q}_y = \{-N_y+1, -N_y+2, \ldots, M_yN_y+M_y-1\}. \quad (15)$$

Thus, a virtual URA $\mathbb{Q} = \{(x_{\mathbb{Q}}, y_{\mathbb{Q}}) | x_{\mathbb{Q}} = \mathbb{Q}_x d, y_{\mathbb{Q}} = \mathbb{Q}_y d\}$ as shown in Fig. 2(b) can be extracted from $\mathbb{D}$ with

$$|\mathbb{Q}_x| = M_xN_x + M_x + N_x - 1,$$

$$|\mathbb{Q}_y| = M_yN_y + M_y + N_y - 1 \quad (16)$$

representing the numbers of virtual sensors in $\mathbb{Q}$ along the x-axis and the y-axis, respectively. By properly extracting elements in $\boldsymbol{R}$ and reorganizing them to map the locations of virtual sensors in the virtual URA $\mathbb{Q}$, the equivalent second-order signal of $\mathbb{Q}$ can be obtained as

$$\boldsymbol{U} = \sum_{k=1}^{K} \sigma_k^2 \boldsymbol{b}(\mu_k) \circ \boldsymbol{b}(\nu_k) + \boldsymbol{Z} \in \mathbb{C}^{|\mathbb{Q}_x| \times |\mathbb{Q}_y|}, \quad (17)$$

where

$$\boldsymbol{b}(\mu_k) =$$

$$\left[e^{-\jmath\pi(-N_x+1)\mu_k}, e^{-\jmath\pi(-N_x+2)\mu_k}, \ldots, e^{-\jmath\pi(M_xN_x+M_x-1)\mu_k} \right]^{\mathrm{T}},$$

$$\boldsymbol{b}(\nu_k) =$$

$$\left[e^{-\jmath\pi(-N_y+1)\nu_k}, e^{-\jmath\pi(-N_y+2)\nu_k}, \ldots, e^{-\jmath\pi(M_yN_y+M_y-1)\nu_k} \right]^{\mathrm{T}}$$

(18)

respectively serve as the steering vectors of $\mathbb{Q}$ along the x-axis and the y-axis, and $\boldsymbol{Z}$ is the corresponding noise term with only the (N_x, N_y)-th element being σ_n^2 while others are 0.

It is known that the size of the derived virtual URA $\mathbb{Q}$ affects the achievable source identifiability for DOA estimation. The optimization problems we design will maximize the number of DOFs, which depends on the size of $\mathbb{Q}$. To ensure that the resulting maximum number of DOFs is an integer, we provide the following remark on the even number property of the size of $\mathbb{Q}$ before proceeding to the derivation of the coarray tensor.

Remark: The size of the virtual URA $\mathbb{Q}$, namely, $|\mathbb{Q}_x|$ and $|\mathbb{Q}_y|$ in (16), can be equivalently expressed as $|\mathbb{Q}_x| = (M_x + 1)(N_x + 1) - 2$ and $|\mathbb{Q}_y| = (M_y + 1)(N_y + 1) - 2$. Since the coprime integers M_x and N_x cannot be even numbers together, there is at least one even number in $M_x + 1$ and $N_x + 1$, which means that $(M_x + 1)(N_x + 1)$ is an even number. Therefore, $|\mathbb{Q}_x|$ is an even number. Likewise, $|\mathbb{Q}_y|$ is also an even number.

Different from the auto-correlation-based virtual array which is symmetric to the coordinate axes due to the Hermitian property of the covariance matrix, the virtual URA $\mathbb{Q}$ derived from the cross-correlation statistics is asymmetric to the coordinate axes [48]. To expand the attainable virtual array aperture, we exploit the mirrored image of $\mathbb{Q}$, i.e., $\tilde{\mathbb{Q}}$, as shown in Fig. 2(b). According to the conjugate symmetry property of the array manifold matrix [49], the coarray signal $\tilde{\boldsymbol{U}} \in \mathbb{C}^{|\mathbb{Q}_x| \times |\mathbb{Q}_y|}$ corresponding to $\tilde{\mathbb{Q}}$ can be obtained by reversing the elements in each dimension of $\boldsymbol{U}^*$ as

$$\tilde{\boldsymbol{U}} = \sum_{k=1}^{K} \sigma_k^2 \left[\boldsymbol{b}(\mu_k) v(\mu_k) \right] \circ \left[\boldsymbol{b}(\nu_k) v(\nu_k) \right] + \tilde{\boldsymbol{Z}}, \quad (19)$$

where

$$v(\mu_k) = e^{-\jmath\pi(-M_xN_x-M_x+N_x)\mu_k},$$

$$v(\nu_k) = e^{-\jmath\pi(-M_yN_y-M_y+N_y)\nu_k} \quad (20)$$

respectively reflect the symmetric projection from $\mathbb{Q}$ to $\tilde{\mathbb{Q}}$ along the x-axis and the y-axis, and $\tilde{\boldsymbol{Z}}$ is the symmetric noise term.

Then, as shown in Fig. 2(c), the virtual URA $\mathbb{Q}$ and its mirrored extension $\tilde{\mathbb{Q}}$ can be piled in the lateral direction to formulate a 3-D virtual uniform cuboid array (UCA) $\mathbb{G}$. Accordingly, concatenating $\boldsymbol{U}$ and $\tilde{\boldsymbol{U}}$ along an additional dimension leads to a coarray tensor $\mathcal{U} \in \mathbb{C}^{|\mathbb{Q}_x| \times |\mathbb{Q}_y| \times 2}$ corresponding to $\mathbb{G}$

as

$$\boldsymbol{\mathcal{U}} = [\boldsymbol{U}, \tilde{\boldsymbol{U}}]_{\sqcup_3} = \sum_{k=1}^{K} \sigma_k^2 \boldsymbol{b}(\mu_k) \circ \boldsymbol{b}(\nu_k) \circ \boldsymbol{v}(k) + \boldsymbol{\mathcal{Z}}$$

$$\triangleq [\![\boldsymbol{\sigma}; \boldsymbol{B}_x, \boldsymbol{B}_y, \boldsymbol{V}]\!] + \boldsymbol{\mathcal{Z}}, \tag{21}$$

where

$$\boldsymbol{v}(k) = [1, v(\mu_k)v(\nu_k)]^{\mathrm{T}} \tag{22}$$

is the symmetric factor, $\boldsymbol{B}_x = [\boldsymbol{b}(\mu_1), \boldsymbol{b}(\mu_2), \dots, \boldsymbol{b}(\mu_K)] \in \mathbb{C}^{|\mathbb{Q}_x| \times K}$, $\boldsymbol{B}_y = [\boldsymbol{b}(\nu_1), \boldsymbol{b}(\nu_2), \dots, \boldsymbol{b}(\nu_K)] \in \mathbb{C}^{|\mathbb{Q}_y| \times K}$, $\boldsymbol{V} = [\boldsymbol{v}(1), \boldsymbol{v}(2), \dots, \boldsymbol{v}(K)] \in \mathbb{C}^{2 \times K}$ are the factor matrices, $\boldsymbol{\sigma} = [\sigma_1^2, \sigma_2^2, \dots, \sigma_K^2]^{\mathrm{T}}$ is the source power vector, and $\boldsymbol{\mathcal{Z}}$ is the noise tensor with the $(N_x, N_y, 1)$-th and $(M_x N_x + M_x, M_y N_y + M_y, 2)$-th elements being σ_n^2 while all others are 0. Note that, following the CP model of sub-Nyquist tensors in (9) and (10), the corresponding coarray tensor in (21) is also represented as a CP model, whose unique decomposability enables the analysis of source identifiability. The other tensor representations, such as the Tucker representation, will cause a problem of model mismatch, and may not be unique when it comes to coarray tensor decomposition.

B. Dimension Increment for Coarray Tensor

Although the virtual UCA $\mathbb{G}$ provides an increased number of virtual sensors compared to the number of physical sensors, the achievable source identifiability for DOA estimation is determined by the uniqueness condition for coarray tensor CPD. In particular, the source identifiability for DOA estimation using direct CPD of the coarray tensor $\boldsymbol{\mathcal{U}}$ conforms to the following proposition.

Proposition: The direct CPD of $\boldsymbol{\mathcal{U}}$ results in a limited number of DOFs, which cannot exceed the number of physical sensors in the coprime planar array $\mathbb{P}$.

Proof: According to (2), the CPD of $\boldsymbol{\mathcal{U}}$ is unique only if

$$\kappa(\boldsymbol{B}_x) + \kappa(\boldsymbol{B}_y) + \kappa(\boldsymbol{V}) \geqslant 2K + 2, \tag{23}$$

where $\kappa(\boldsymbol{B}_x) = \min(|\mathbb{Q}_x|, K)$, $\kappa(\boldsymbol{B}_y) = \min(|\mathbb{Q}_y|, K)$, and $\kappa(\boldsymbol{V}) = \min(2, K)$. When $K \geqslant \max(|\mathbb{Q}_x|, |\mathbb{Q}_y|)$, we can substitute $\kappa(\boldsymbol{B}_x) = |\mathbb{Q}_x|$, $\kappa(\boldsymbol{B}_y) = |\mathbb{Q}_y|$, and $\kappa(\boldsymbol{V}) = 2$ into (23), leading to $(|\mathbb{Q}_x| + |\mathbb{Q}_y|)/2 \geqslant K \geqslant \max(|\mathbb{Q}_x|, |\mathbb{Q}_y|)$, which is infeasible except for $|\mathbb{Q}_x| = |\mathbb{Q}_y|$. In that case, we have $|\mathbb{P}| > K = |\mathbb{Q}_x| = |\mathbb{Q}_y|$. When $|\mathbb{Q}_y| \geqslant K \geqslant |\mathbb{Q}_x|$, substituting $\kappa(\boldsymbol{B}_x) = |\mathbb{Q}_x|$ and $\kappa(\boldsymbol{B}_y) = K$ into (23) yields $|\mathbb{P}| > |\mathbb{Q}_x| \geqslant K$. Likewise, when $|\mathbb{Q}_x| \geqslant K \geqslant |\mathbb{Q}_y|$, we have $|\mathbb{P}| > |\mathbb{Q}_y| \geqslant K$ by substituting $\kappa(\boldsymbol{B}_x) = K$ and $\kappa(\boldsymbol{B}_y) = |\mathbb{Q}_y|$ into (23). The above analysis indicates that the achievable number of DOFs for the direct CPD of $\boldsymbol{\mathcal{U}}$ cannot exceed the number of physical sensors. ■

Based on the *Proposition*, a dimension increment approach is designed for the coarray tensor to embed additional spatial information, which offers the opportunity to refine the coarray tensor structure. As a result, the Kruskal's ranks of the refined coarray tensor's CP factors can be increased for enhancing the source identifiability. To be specific, a sub-coarray tensor $\boldsymbol{\mathcal{U}}_{(1,1)} \in \mathbb{C}^{P_x \times P_y \times 2}$ can be obtained by extracting elements from

$\boldsymbol{\mathcal{U}}$ with a segmentation window of size $P_x \times P_y$, i.e., $\boldsymbol{\mathcal{U}}_{(1,1)} = \boldsymbol{\mathcal{U}}(-N_x + 1 : -N_x + P_x, -N_y + 1 : -N_y + P_y, 1 : 2)$. Then, as shown in Fig. 3(a), the segmentation window is sequentially shifted along the x-axis and the y-axis, which yields $L_x L_y$ sub-coarray tensors

$$\boldsymbol{\mathcal{U}}_{(l_x, l_y)} = \boldsymbol{\mathcal{U}}(-N_x + l_x : -N_x + P_x + l_x - 1,$$
$$-N_y + l_y : -N_y + P_y + l_y - 1, 1 : 2) \tag{24}$$

of size $P_x \times P_y \times 2$ for $l_x = 1, 2, \dots, L_x$ and $l_y = 1, 2, \dots, L_y$. Here,

$$L_x = |\mathbb{Q}_x| + 1 - P_x,$$
$$L_y = |\mathbb{Q}_y| + 1 - P_y \tag{25}$$

respectively denote the number of sub-coarray tensors along the x-axis and the y-axis. To ensure that the numbers of sub-coarray tensors satisfy $2 \leqslant L_x \leqslant |\mathbb{Q}_x| - 1$ and $2 \leqslant L_y \leqslant |\mathbb{Q}_y| - 1$, we have

$$2 \leqslant P_x \leqslant |\mathbb{Q}_x| - 1,$$
$$2 \leqslant P_y \leqslant |\mathbb{Q}_y| - 1. \tag{26}$$

The sub-coarray tensor $\boldsymbol{\mathcal{U}}_{(l_x, l_y)}$ can be expressed as

$$\boldsymbol{\mathcal{U}}_{(l_x, l_y)} = \boldsymbol{\mathcal{U}} \times_1 \boldsymbol{S}_{l_x} \times_2 \boldsymbol{S}_{l_y}, \tag{27}$$

where

$$\boldsymbol{S}_{l_x} = \left[\boldsymbol{0}_{P_x \times (l_x - 1)}, \boldsymbol{I}_{P_x \times P_x}, \boldsymbol{0}_{P_x \times (|\mathbb{Q}_x| - P_x - l_x + 1)}\right]^{\mathrm{T}} \in \mathbb{C}^{|\mathbb{Q}_x| \times P_x},$$

$$\boldsymbol{S}_{l_y} = \left[\boldsymbol{0}_{P_y \times (l_y - 1)}, \boldsymbol{I}_{P_y \times P_y}, \boldsymbol{0}_{P_y \times (|\mathbb{Q}_y| - P_y - l_y + 1)}\right]^{\mathrm{T}} \in \mathbb{C}^{|\mathbb{Q}_y| \times P_y} \tag{28}$$

are segmentation matrices along the x-axis and the y-axis, respectively.

Since the $L_x L_y$ sub-coarray tensors $\boldsymbol{\mathcal{U}}_{(l_x, l_y)}$ with adjacent indices l_x and l_y respectively present a shifting relationship along the x-axis and the y-axis, a shifting-embedded coarray tensor can be constructed from concatenating these sub-coarray tensors as shown in Fig. 3(b). Specifically, the L_x sub-coarray tensors $\boldsymbol{\mathcal{U}}_{(:, l_y)}$ for a given index l_y share the same angular information along the y-axis but own a one-step shifting relationship along the x-axis. Thus, they are concatenated along an additional shifting dimension to generate a 4-D tensor

$$\bar{\boldsymbol{\mathcal{U}}}_{(l_y)} = [\boldsymbol{\mathcal{U}}_{(1, l_y)}, \boldsymbol{\mathcal{U}}_{(2, l_y)}, \cdots, \boldsymbol{\mathcal{U}}_{(L_x, l_y)}]_{\sqcup_4} \in \mathbb{C}^{P_x \times P_y \times 2 \times L_x},$$
$$\forall l_y = 1, 2, \dots, L_y. \tag{29}$$

Since the L_y 4-D tensors $\{\bar{\boldsymbol{\mathcal{U}}}_{(l_y)}, l_y = 1, 2, \dots, L_y\}$ present a one-step shifting relationship along the y-axis, they are further concatenated to formulate a five-dimensional (5-D) shifting-embedded coarray tensor

$$\boldsymbol{\mathcal{H}} = [\bar{\boldsymbol{\mathcal{U}}}_{(1)}, \bar{\boldsymbol{\mathcal{U}}}_{(2)}, \cdots, \bar{\boldsymbol{\mathcal{U}}}_{(L_y)}]_{\sqcup_5} \in \mathbb{C}^{P_x \times P_y \times 2 \times L_x \times L_y}$$

$$= \sum_{k=1}^{K} \sigma_k^2 \boldsymbol{c}(\mu_k) \circ \boldsymbol{c}(\nu_k) \circ \boldsymbol{v}(k) \circ \boldsymbol{g}(\mu_k) \circ \boldsymbol{g}(\nu_k) + \bar{\boldsymbol{\mathcal{Z}}}$$

$$\triangleq [\![\boldsymbol{\sigma}; \boldsymbol{C}_x, \boldsymbol{C}_y, \boldsymbol{V}, \boldsymbol{G}_x, \boldsymbol{G}_y]\!] + \bar{\boldsymbol{\mathcal{Z}}}, \tag{30}$$
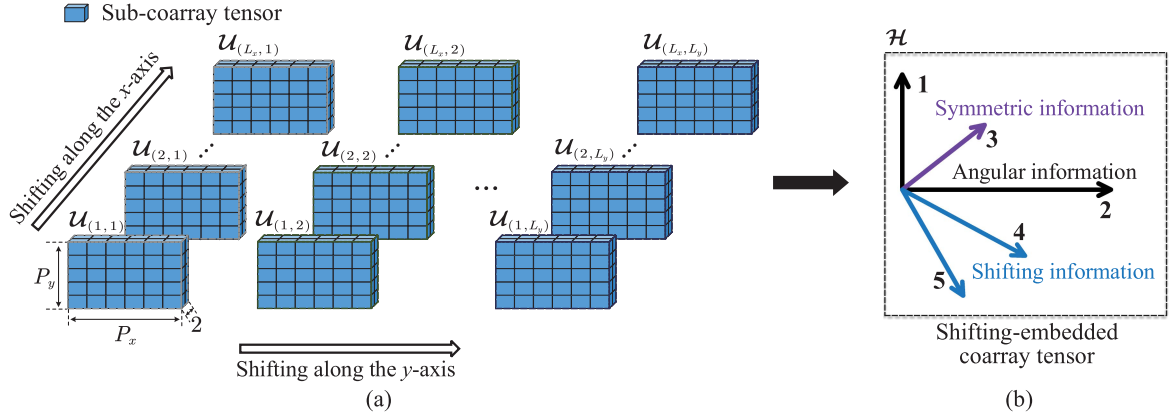
Fig. 3. Illustration of the dimension increment operation on the coarray tensor. (a) The segmented sub-coarray tensors $\mathcal{U}_{(l_x, l_y)}$. (b) The shifting-embedded coarray tensor $\mathcal{H}$.

where

$$c(\mu_k) =$$

$$\left[e^{-\jmath\pi(-N_x+1)\mu_k}, e^{-\jmath\pi(-N_x+2)\mu_k}, \cdots, e^{-\jmath\pi(-N_x+P_x)\mu_k} \right]^{\mathrm{T}},$$

$$c(\nu_k) =$$

$$\left[e^{-\jmath\pi(-N_y+1)\nu_k}, e^{-\jmath\pi(-N_y+2)\nu_k}, \cdots, e^{-\jmath\pi(-N_y+P_y)\nu_k} \right]^{\mathrm{T}} \quad (31)$$

are respectively angular factors along the x-axis and the y-axis,

$$g(\mu_k) = [1, e^{-\jmath\pi\mu_k}, \ldots, e^{-\jmath\pi(L_x-1)\mu_k}]^{\mathrm{T}},$$

$$g(\nu_k) = [1, e^{-\jmath\pi\nu_k}, \ldots, e^{-\jmath\pi(L_y-1)\nu_k}]^{\mathrm{T}} \quad (32)$$

are respectively shifting factors along the x-axis and the y-axis, $\boldsymbol{C}_x = [\boldsymbol{c}(\mu_1), \ \boldsymbol{c}(\mu_2), \ldots, \ \boldsymbol{c}(\mu_K)] \in \mathbb{C}^{P_x \times K}$, $\boldsymbol{C}_y = [\boldsymbol{c}(\nu_1), \boldsymbol{c}(\nu_2), \ldots, \boldsymbol{c}(\nu_K)] \in \mathbb{C}^{P_y \times K}$, $\boldsymbol{G}_x = [\boldsymbol{g}(\mu_1), \boldsymbol{g}(\mu_2), \ldots, \boldsymbol{g}(\mu_K)] \in \mathbb{C}^{L_x \times K}$, $\boldsymbol{G}_y = [\boldsymbol{g}(\nu_1), \boldsymbol{g}(\nu_2), \ldots, \boldsymbol{g}(\nu_K)] \in \mathbb{C}^{L_y \times K}$ are the corresponding CP factor matrices, and $\bar{\mathcal{Z}}$ is the noise tensor.

Obviously, the five dimensions of the shifting-embedded coarray tensor $\mathcal{H}$ can be categorized into the angular dimensions along the x, y-axes, the symmetric dimension, and the shifting dimensions along the x, y-axes. This enables us to structurally combine the dimensions of $\mathcal{H}$ to formulate a new coarray tensor with augmented CP factors, which contributes to the enhanced source identifiability. More importantly, by finding the optimal coarray tensor structure related to the maximum number of DOFs, the underdetermined DOA estimation can be achieved.

V. UNDERDETERMINED DOA ESTIMATION

In this section, we develop an optimal strategy to reshape the shifting-embedded coarray tensor to enhance the source identifiability. The resulting coarray tensor with the optimal structure can then be decomposed for underdetermined DOA estimation.

A. Identifiability Enhancement: Directionally Reshaping

Based on the rule of generalized tensor reshaping of the CP model, properly reshaping the shifting-embedded coarray tensor $\mathcal{H}$ increases the Kruskal's ranks of the resulting tensor's CP factors. As such, a directionally reshaping approach is designed as the first identifiability enhancement strategy.

In particular, since the dimension sets $\{1, 4\}$, $\{2, 5\}$, and $\{3\}$ of $\mathcal{H}$ respectively represent spatial information in the azimuthal, vertical, and lateral directions, it can be reshaped as

$$\mathcal{K}_{\mathrm{d}} \triangleq \langle \mathcal{H} \rangle_{\{1,4\},\{2,5\},\{3\}} \in \mathbb{C}^{P_x L_x \times P_y L_y \times 2}$$

$$= \sum_{k=1}^{K} \sigma_k^2 \boldsymbol{f}(\mu_k) \circ \boldsymbol{f}(\nu_k) \circ \boldsymbol{v}(k) + \mathcal{Q}_{\mathrm{d}}$$

$$\triangleq [\![\boldsymbol{\sigma}; \boldsymbol{F}_x, \boldsymbol{F}_y, \boldsymbol{V}]\!] + \mathcal{Q}_{\mathrm{d}}, \quad (33)$$

where

$$\boldsymbol{f}(\mu_k) = \boldsymbol{g}(\mu_k) \otimes \boldsymbol{c}(\mu_k) \in \mathbb{C}^{P_x L_x},$$

$$\boldsymbol{f}(\nu_k) = \boldsymbol{g}(\nu_k) \otimes \boldsymbol{c}(\nu_k) \in \mathbb{C}^{P_y L_y} \quad (34)$$

are directional factors, $\boldsymbol{F}_x = [\boldsymbol{f}(\mu_1), \boldsymbol{f}(\mu_2), \cdots, \boldsymbol{f}(\mu_K)] = \boldsymbol{G}_x \odot \boldsymbol{C}_x \in \mathbb{C}^{P_x L_x \times K}$, $\boldsymbol{F}_y = [\boldsymbol{f}(\nu_1), \boldsymbol{f}(\nu_2), \cdots, \boldsymbol{f}(\nu_K)] = \boldsymbol{G}_y \odot \boldsymbol{C}_y \in \mathbb{C}^{P_y L_y \times K}$ are the corresponding directional factor matrices, and $\mathcal{Q}_{\mathrm{d}}$ is the directionally reshaped noise tensor. The directional factors can be retrieved from the CPD of the directionally reshaped coarray tensor $\mathcal{K}_{\mathrm{d}}$ (33) for DOA estimation, and the source identifiability obeys the following property.

Theorem 1: The source identifiability of decomposing the directionally reshaped coarray tensor $\mathcal{K}_{\mathrm{d}}$ can be given by

$$\mathrm{DOF}_{\mathrm{d}} = [\min(|\mathbb{Q}_x|, |\mathbb{Q}_y|)(\min(|\mathbb{Q}_x|, |\mathbb{Q}_y|) + 2)]/4. \quad (35)$$

Proof: The CPD of $\mathcal{K}_{\mathrm{d}}$ is unique if

$$\kappa(\boldsymbol{F}_x) + \kappa(\boldsymbol{F}_y) + \kappa(\boldsymbol{V}) \geqslant 2K + 2. \quad (36)$$

Based on the Kruskal's rank of the Khatri-Rao product [50], we have

$$\min(P_x L_x, K) \geqslant \kappa(\boldsymbol{F}_x) \geqslant \min\left(\kappa(\boldsymbol{G}_x) + \kappa(\boldsymbol{C}_x) - 1, K\right),$$
$$\min(P_y L_y, K) \geqslant \kappa(\boldsymbol{F}_y) \geqslant \min\left(\kappa(\boldsymbol{G}_y) + \kappa(\boldsymbol{C}_y) - 1, K\right),$$
$$(37)$$

where $\kappa(\boldsymbol{G}_x) = \min(L_x, K)$, $\kappa(\boldsymbol{C}_x) = \min(P_x, K)$, $\kappa(\boldsymbol{G}_y) = \min(L_y, K)$, and $\kappa(\boldsymbol{C}_y) = \min(P_y, K)$.

When $K \geqslant \max(P_x L_x, P_y L_y)$, the inequality (36) can be transformed into $(P_x L_x + P_y L_y)/2 \geqslant K \geqslant P_x L_x, P_y L_y$, which leads to $P_x(|\mathbb{Q}_x| + 1 - P_x) = P_y(|\mathbb{Q}_y| + 1 - P_y)$. For an arbitrary coprime planar array geometry, $|\mathbb{Q}_x|$ is not necessarily equal to $|\mathbb{Q}_y|$, implying $P_x(|\mathbb{Q}_x| + 1 - P_x) \neq P_y(|\mathbb{Q}_y| + 1 - P_y)$. Therefore, there is no feasible solution under the condition of $K \geqslant \max(P_x L_x, P_y L_y)$. When $P_x L_x \geqslant K \geqslant P_y L_y$, we derive the following relationship

$$K = P_y L_y = P_y(|\mathbb{Q}_y| + 1 - P_y). \quad (38)$$

As such, a quadratic programming problem

$$\max_{P_y} \quad P_y(|\mathbb{Q}_y| + 1 - P_y)$$
$$\text{s.t.} \quad P_y \leqslant |\mathbb{Q}_y| - 1, \quad (39)$$

is designed to maximize K, and the solution becomes $P_y = (|\mathbb{Q}_y| + 1)/2$. According to the *Remark* in Subsection IV-A, $|\mathbb{Q}_y|$ is an even number, making $(|\mathbb{Q}_y| + 1)/2$ a non-integer. Thus, the optimal value of P_y is set to

$$P_y = |\mathbb{Q}_y|/2, \quad (40)$$

such that the maximum value of K (38) is $[|\mathbb{Q}_y|(|\mathbb{Q}_y| + 2)]/4$. Likewise, when $P_y L_y \geqslant K \geqslant P_x L_x$, P_x can be optimized as

$$P_x = |\mathbb{Q}_x|/2, \quad (41)$$

leading to $K = P_x(|\mathbb{Q}_x| + 1 - P_x) = [|\mathbb{Q}_x|(|\mathbb{Q}_x| + 2)]/4$. As a result, the maximum number of DOFs for the directionally reshaping approach can be represented as $\text{DOF}_d = [\min(|\mathbb{Q}_x|, |\mathbb{Q}_y|)(\min(|\mathbb{Q}_x|, |\mathbb{Q}_y|) + 2)]/4$ as in (35). ∎

Note that, when the deployed coprime planar array $\mathbb{P}$ has a relatively large size along the y-axis or the x-axis, we have $|\mathbb{Q}_y| \gg |\mathbb{Q}_x|$ or $|\mathbb{Q}_x| \gg |\mathbb{Q}_y|$. In either case, the resulting number of DOFs $[|\mathbb{Q}_x|(|\mathbb{Q}_x| + 2)]/4$ or $[|\mathbb{Q}_y|(|\mathbb{Q}_y| + 2)]/4$ will be much smaller than the number of physical sensors $|\mathbb{P}|$.

B. Identifiability Enhancement: Spatially Reshaping

To address the issue of limited source identifiability, we propose a spatially reshaping approach as another identifiability enhancement strategy. It combines the dimensions of the shifting-embedded coarray tensor $\mathcal{H}$ that represent the same category of spatial information. Specifically, considering that the dimension sets $\{1, 2\}$, $\{4, 5\}$, and $\{3\}$ respectively represent the angular, shifting, and symmetric information, $\mathcal{H}$ can be reshaped as

$$\mathcal{K}_s \triangleq \langle\mathcal{H}\rangle_{\{1,2\},\{4,5\},\{3\}} \in \mathbb{C}^{P_x P_y \times L_x L_y \times 2}$$

$$= \sum_{k=1}^{K} \sigma_k^2 \boldsymbol{c}(k) \circ \boldsymbol{g}(k) \circ \boldsymbol{v}(k) + \mathcal{Q}_s$$
$$\triangleq [\![\boldsymbol{\sigma}; \boldsymbol{C}, \boldsymbol{G}, \boldsymbol{V}]\!] + \mathcal{Q}_s, \quad (42)$$

where

$$\boldsymbol{c}(k) = \boldsymbol{c}(\nu_k) \otimes \boldsymbol{c}(\mu_k) \in \mathbb{C}^{P_x P_y},$$
$$\boldsymbol{g}(k) = \boldsymbol{g}(\nu_k) \otimes \boldsymbol{g}(\mu_k) \in \mathbb{C}^{L_x L_y} \quad (43)$$

are spatial factors, $\boldsymbol{C} = [\boldsymbol{c}(1), \boldsymbol{c}(2), \ldots, \boldsymbol{c}(K)] = \boldsymbol{C}_y \odot \boldsymbol{C}_x \in \mathbb{C}^{P_x P_y \times K}$, $\boldsymbol{G} = [\boldsymbol{g}(1), \boldsymbol{g}(2), \ldots, \boldsymbol{g}(K)] = \boldsymbol{G}_y \odot \boldsymbol{G}_x \in \mathbb{C}^{L_x L_y \times K}$ are the corresponding spatial factor matrices, and $\mathcal{Q}_s$ is the spatially reshaped noise tensor. The source identifiability of this approach obeys the following property.

Theorem 2: The source identifiability of decomposing the spatially reshaped coarray tensor $\mathcal{K}_s$ can be given by

$$\text{DOF}_s = [\min(|\mathbb{Q}_x|, |\mathbb{Q}_y|)(\max(|\mathbb{Q}_x|, |\mathbb{Q}_y|) + 2)]/4, \quad (44)$$

which is larger than the number of physical sensors in the coprime planar array $\mathbb{P}$.

Proof: The CPD of $\mathcal{K}_s$ is unique if

$$\kappa(\boldsymbol{C}) + \kappa(\boldsymbol{G}) + \kappa(\boldsymbol{V}) \geqslant 2K + 2, \quad (45)$$

where

$$\min(P_x P_y, K) \geqslant \kappa(\boldsymbol{C}) \geqslant \min\left(\kappa(\boldsymbol{C}_y) + \kappa(\boldsymbol{C}_x) - 1, K\right),$$
$$\min(L_x L_y, K) \geqslant \kappa(\boldsymbol{G}) \geqslant \min\left(\kappa(\boldsymbol{G}_y) + \kappa(\boldsymbol{G}_x) - 1, K\right).$$
$$(46)$$

When $K \geqslant \max(P_x P_y, L_x L_y)$, substituting $P_x P_y \geqslant \kappa(\boldsymbol{C}) \geqslant P_x + P_y - 1$, $L_x L_y \geqslant \kappa(\boldsymbol{G}) \geqslant L_x + L_y - 1$, and $\kappa(\boldsymbol{V}) = 2$ into (45) yields

$$(P_x P_y + L_x L_y)/2 \geqslant K \geqslant P_x P_y, L_x L_y, \quad (47)$$

which leads to $P_x P_y = L_x L_y$. The inequality (47) is equivalent to

$$[P_x P_y + (|\mathbb{Q}_x| + 1 - P_x)(|\mathbb{Q}_y| + 1 - P_y)]/2 \geqslant K, \quad (48)$$

such that K can be maximized through the following segmentation window size optimization problem

$$\max_{P_x, P_y} \quad P_x P_y + (|\mathbb{Q}_x| + 1 - P_x)(|\mathbb{Q}_y| + 1 - P_y)$$
$$\text{s.t.} \quad P_x \leqslant |\mathbb{Q}_x| - 1,$$
$$P_y \leqslant |\mathbb{Q}_y| - 1. \quad (49)$$

Using the Lagrange multiplier algorithm to solve (49), the optimal $\{P_x, P_y\}$ can be obtained as

$$P_x = (|\mathbb{Q}_x| + 1)/2,$$
$$P_y = (|\mathbb{Q}_y| + 1)/2. \quad (50)$$

The details of solving (49) can be found in Appendix A. Since P_x and P_y must be integers, they can be either rounded up or down to integers. However, the rounding of $\{P_x, P_y\}$ in (50) cannot satisfy $P_x P_y = L_x L_y$. Therefore, there is no feasible solution under the condition of $K \geqslant \max(P_x P_y, L_x L_y)$.

Furthermore, when $L_x L_y \geqslant K \geqslant P_x P_y$, we have

$$\begin{cases} K + P_x P_y + 2 \geqslant 2K + 2, \\ K \geqslant P_x P_y, \end{cases} \tag{51}$$

leading to $K = P_x P_y$. Thus, the maximum value of K can be obtained from

$$\begin{aligned} \max_{P_x, P_y} \quad & P_x P_y \\ \text{s.t.} \quad & P_x \leqslant |\mathbb{Q}_x| - 1, \\ & P_y \leqslant |\mathbb{Q}_y| - 1, \\ & P_x P_y \leqslant (|\mathbb{Q}_x| + 1 - P_x)(|\mathbb{Q}_y| + 1 - P_y), \end{aligned} \tag{52}$$

which is also solved by the Lagrange multiplier algorithm. The details of solving (52) can be found in Appendix B. Although the optimal solution $\{P_x, P_y\}$ in (52) is the same as that of (50), (52) does not require the constraint $P_x P_y = L_x L_y$. As such, we can set $\{P_x, P_y\}$ to

$$\{P_x, P_y\} = \begin{cases} \{|\mathbb{Q}_x|/2, (|\mathbb{Q}_y| + 2)/2\} & |\mathbb{Q}_x| < |\mathbb{Q}_y|, \\ \{(|\mathbb{Q}_x| + 2)/2, |\mathbb{Q}_y|/2\} & |\mathbb{Q}_x| \geqslant |\mathbb{Q}_y|, \end{cases} \tag{53}$$

where $L_x L_y \geqslant P_x P_y$ can be satisfied. Likewise, when $P_x P_y \geqslant K \geqslant L_x L_y$, we obtain the same solution as (53). Therefore, the maximum number of DOFs for the spatially reshaping approach is $\mathrm{DOF_s} = [\min(|\mathbb{Q}_x|, |\mathbb{Q}_y|)(\max(|\mathbb{Q}_x|, |\mathbb{Q}_y|) + 2)]/4.$ ∎

Compared to the achievable source identifiability for the directionally reshaping approach in (35), it is clear that $\mathrm{DOF_s} \geqslant \mathrm{DOF_d}$. More importantly, the source identifiability for the spatially reshaping approach given in (44) is higher than the number of physical sensors $|\mathbb{P}|$, i.e.,

$$\mathrm{DOF_s} > 4 M_x M_y + N_x N_y - 1. \tag{54}$$

As such, by adopting the spatially reshaping approach to refine the coarray tensor structure, it is guaranteed that the underdetermined DOA estimation can be achieved with the optimal source identifiability. It is worth mentioning that, for generalized coprime planar array DOA estimation exploiting the typical array decomposition approach [51], the maximum number of DOFs is $\min(4 M_x M_y, N_x N_y) - 1$, which is smaller than that of the proposed algorithm.

C. Optimally Reshaped Coarray Tensor CPD

To achieve 2-D DOA estimation for the coprime planar array, the spatially reshaped coarray tensor $\boldsymbol{\mathcal{K}}_s$ is decomposed via CPD to obtain the estimated factor matrices $\hat{\boldsymbol{C}} = [\hat{\boldsymbol{c}}(1), \hat{\boldsymbol{c}}(2), \dots, \hat{\boldsymbol{c}}(K)]$, $\hat{\boldsymbol{G}} = [\hat{\boldsymbol{g}}(1), \hat{\boldsymbol{g}}(2), \dots, \hat{\boldsymbol{g}}(K)]$, and $\hat{\boldsymbol{V}} = [\hat{\boldsymbol{v}}(1), \hat{\boldsymbol{v}}(2), \dots, \hat{\boldsymbol{v}}(K)]$, where $\hat{\boldsymbol{c}}(k)$, $\hat{\boldsymbol{g}}(k)$, and $\hat{\boldsymbol{v}}(k)$ are the estimated spatial factors of $\boldsymbol{\mathcal{K}}_s$.

Specifically, the CPD of $\boldsymbol{\mathcal{K}}_s$ can be characterized by the following least square optimization problem

$$\left\{ \hat{\boldsymbol{C}}, \hat{\boldsymbol{G}}, \hat{\boldsymbol{V}} \right\} = \arg\min_{\hat{\boldsymbol{C}}, \hat{\boldsymbol{G}}, \hat{\boldsymbol{V}}} \left\| \boldsymbol{\mathcal{K}}_s - \left[\!\left[\boldsymbol{\sigma}; \hat{\boldsymbol{C}}, \hat{\boldsymbol{G}}, \hat{\boldsymbol{V}} \right]\!\right] \right\|_{\mathrm{F}}. \tag{55}$$

The above coarray tensor CPD problem[2] can be solved by the trilinear alternating least square algorithm, which iteratively updates the estimated factor matrices as

$$\hat{\boldsymbol{C}} = \arg\min_{\hat{\boldsymbol{C}}} \left\| [\boldsymbol{\mathcal{K}}_s]_1 - \hat{\boldsymbol{C}} \left(\hat{\boldsymbol{V}} \odot \hat{\boldsymbol{G}} \right)^{\mathrm{T}} \right\|_{\mathrm{F}}^2,$$

$$\hat{\boldsymbol{G}} = \arg\min_{\hat{\boldsymbol{G}}} \left\| [\boldsymbol{\mathcal{K}}_s]_2 - \hat{\boldsymbol{G}} \left(\hat{\boldsymbol{V}} \odot \hat{\boldsymbol{C}} \right)^{\mathrm{T}} \right\|_{\mathrm{F}}^2,$$

$$\hat{\boldsymbol{V}} = \arg\min_{\hat{\boldsymbol{V}}} \left\| [\boldsymbol{\mathcal{K}}_s]_3 - \hat{\boldsymbol{V}} \left(\hat{\boldsymbol{G}} \odot \hat{\boldsymbol{C}} \right)^{\mathrm{T}} \right\|_{\mathrm{F}}^2. \tag{56}$$

At each iteration, $\{\hat{\boldsymbol{C}}, \hat{\boldsymbol{G}}, \hat{\boldsymbol{V}}\}$ can be updated in closed-form expressions as

$$\hat{\boldsymbol{C}} = [\boldsymbol{\mathcal{K}}_s]_1 \left(\left(\hat{\boldsymbol{V}} \odot \hat{\boldsymbol{G}} \right)^{\mathrm{T}} \right)^{\dagger},$$

$$\hat{\boldsymbol{G}} = [\boldsymbol{\mathcal{K}}_s]_2 \left(\left(\hat{\boldsymbol{V}} \odot \hat{\boldsymbol{C}} \right)^{\mathrm{T}} \right)^{\dagger},$$

$$\hat{\boldsymbol{V}} = [\boldsymbol{\mathcal{K}}_s]_3 \left(\left(\hat{\boldsymbol{G}} \odot \hat{\boldsymbol{C}} \right)^{\mathrm{T}} \right)^{\dagger}. \tag{57}$$

According to the Kronecker structures of the spatial factors $\boldsymbol{c}(k)$ and $\boldsymbol{g}(k)$ in (43), the estimated directional parameters $\hat{\mu}_k$ and $\hat{\nu}_k$ can be obtained as

$$\hat{\mu}_k =$$

$$\frac{\sum_{\iota_1} \angle(\hat{\boldsymbol{c}}_{(\iota_1+1)}(k)/\hat{\boldsymbol{c}}_{(\iota_1)}(k)) + \sum_{\varsigma_1} \angle(\hat{\boldsymbol{g}}_{(\varsigma_1+1)}(k)/\hat{\boldsymbol{g}}_{(\varsigma_1)}(k))}{(P_x P_y - P_y + L_x L_y - L_y)\pi},$$

$$\hat{\nu}_k =$$

$$\frac{\sum_{\iota_2} \angle(\hat{\boldsymbol{c}}_{(\iota_2+P_x)}(k)/\hat{\boldsymbol{c}}_{(\iota_2)}(k)) + \sum_{\varsigma_2} \angle(\hat{\boldsymbol{g}}_{(\varsigma_2+L_x)}(k)/\hat{\boldsymbol{g}}_{(\varsigma_2)}(k))}{(P_x P_y - P_x + L_x L_y - L_x)\pi},$$

$$\tag{58}$$

$\forall \iota_1 \in \{[1, P_x P_y], \mathrm{mod}(\iota_1, P_y) \neq 0\}$, $\forall \varsigma_1 \in \{[1, L_x L_y], \mathrm{mod}(\varsigma_1, L_y) \neq 0\}$, $\forall \iota_2 \in [1, P_x P_y - P_x]$, $\forall \varsigma_2 \in [1, L_x L_y - L_x]$. Finally, according to the relationship between (θ_k, ϕ_k) and (μ_k, ν_k) established in (6), the closed-form solution to the azimuth and elevation of the k-th source can be obtained as[3]

$$\hat{\theta}_k = \arctan(\hat{\nu}_k / \hat{\mu}_k),$$

$$\hat{\phi}_k = \arcsin\left(\sqrt{\hat{\mu}_k^2 + \hat{\nu}_k^2} \right). \tag{59}$$

---

[2]Note that, the high-order singular value decomposition (HOSVD) can also be applied to decompose the optimally reshaped coarray tensor $\boldsymbol{\mathcal{K}}_s$ and obtain tensor-based signal and noise subspaces. Based on that, the HOSVD-based spectrum can be generated, which yields the estimated source DOAs by searching for the spectral peaks. However, without a closed-form expression, such operation is more time-consuming. In this regard, we prefer to execute CPD of $\boldsymbol{\mathcal{K}}_s$ for DOA estimation.

[3]Similar to the CPD of $\boldsymbol{\mathcal{K}}_s$, the directionally reshaped coarray tensor $\boldsymbol{\mathcal{K}}_d$ can also be decomposed to estimate its factor matrices $\{\hat{\boldsymbol{F}}_x, \hat{\boldsymbol{F}}_y, \hat{\boldsymbol{V}}\}$, from which $(\hat{\mu}_k, \hat{\nu}_k)$ can be retrieved according to the Kronecker structures given in (34) for DOA estimation.
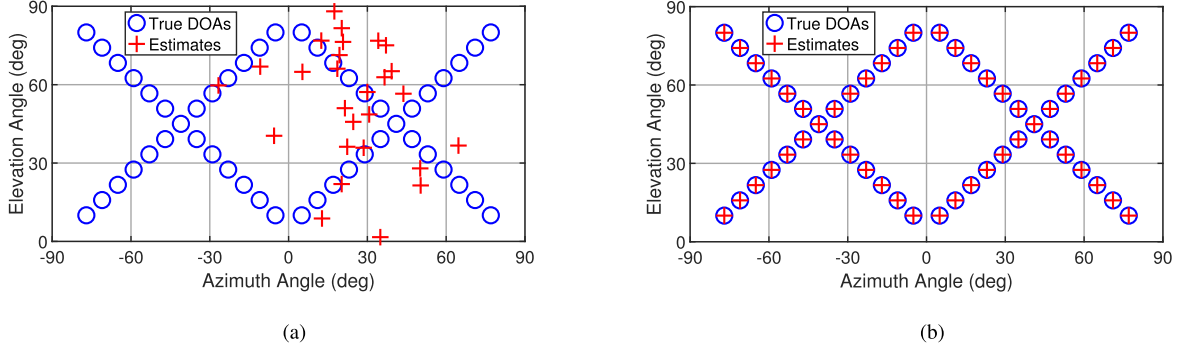
Fig. 4. Source identifiability of the proposed algorithm with 50 sources. (a) The directionally reshaping approach. (b) The spatially reshaping approach.

VI. SIMULATION RESULTS

In the simulations, we deploy a coprime planar array with $M_x = 2$, $M_y = 3$, $N_x = 3$, and $N_y = 4$. Hence, the total number of the sensors is 35. Accordingly, the virtual UCA $\mathbb{G}$ has a size of $10 \times 18 \times 2$, where $|\mathbb{Q}_x| = 10$ and $|\mathbb{Q}_y| = 18$. Since $|\mathbb{Q}_x| < |\mathbb{Q}_y|$, the segmentation window size $\{P_x, P_y\}$ is optimized as $\{5, 10\}$ for both the directionally reshaping approach and the spatially reshaping approach according to (41) and (53), respectively. As such, the directionally reshaped coarray tensor $\mathcal{K}_d$ and the spatially reshaped coarray tensor $\mathcal{K}_s$ have sizes of $30 \times 90 \times 2$ and $50 \times 54 \times 2$, and the corresponding source identifiability is $\text{DOF}_d = 30$ and $\text{DOF}_s = 50$ according to (35) and (44), respectively. It is obvious that the source identifiability for the directionally reshaping approach does not exceed the number of physical sensors in the coprime planar array, i.e., $\text{DOF}_d = 30 < 35$. In contrast, the optimal source identifiability for the spatially reshaping approach does become larger than the number of physical sensors in the coprime planar array, i.e., $\text{DOF}_s = 50 > 35$. In the following simulations, the number of snapshots is fixed at $T = 300$, while the signal-to-noise ratios (SNRs) of source signals are set to 0 dB unless otherwise specified. For each simulated data point, $N_{\text{MC}} = 1,000$ Monte Carlo trials are run. For the proposed algorithm, the dimension increment, reshaping, and decomposition operations on the coarray tensor are implemented with Tensorlab 3.0 [52].

As demonstrated above, we only adopt sub-Nyquist spatial sampling with the coprime planar array, while the temporal sampling rate conforms to the Nyquist-Shannon theorem to provide multiple snapshots. Meanwhile, the setting of the carrier frequency will not influence our proposed sub-Nyquist tensor model in (9) and (10), where the value of carrier frequency in the steering vectors (5) and (7) is offset by the unit inter-element spacing d equaling to half of the signal wavelength.

A. Effectiveness of Coarray Tensor Reshaping for Underdetermined DOA Estimation

To validate the enhanced source identifiability of the proposed coarray tensor DOA estimation algorithm, the result of underdetermined DOA estimation for $K = 50$ sources using different coarray tensor reshaping approaches is presented in Fig. 4. The azimuth angles of the 50 sources are uniformly

distributed in $[-80°, -10°] \cup [10°, 80°]$, while their elevation angles are uniformly distributed in $[10°, 80°]$. In this example, an infinite number of noise-free snapshots are used to provide an ideal modeling for the coarray tensor statistics.

It is clear in Fig. 4(a) that the directionally reshaping approach for coarray tensor fails to estimate these 50 sources because of the limited source identifiability as claimed in *Theorem 1*. In contrast, by using the spatially reshaping approach for coarray tensor refinement, the proposed algorithm is capable of locating all the 50 sources as shown in Fig. 4(b). This result verifies the effectiveness of the proposed algorithm in estimating more sources than the number of physical sensor as claimed in *Theorem 2*, which is benefited from the optimally designed coarray tensor structure with the best source identifiability.

B. Estimation Accuracy of the Proposed Algorithm With Different Coarray Tensor Structures

We now present the estimation accuracy of the proposed algorithm with different coarray tensor structures in Fig. 5, where $K = 2$ sources from directions $(\theta_1, \phi_1) = (34.8°, 26.8°)$ and $(\theta_2, \phi_2) = (45.6°, 38.6°)$ are considered. In particular, the 5-D shifting-embedded coarray tensor $\mathcal{H}$, the directionally reshaping coarray tensor $\mathcal{K}_d$, and the spatially reshaping coarray tensor $\mathcal{K}_s$ are respectively decomposed for DOA estimation. The root-mean-square error (RMSE), defined as

$$\text{RMSE} = \sqrt{\frac{1}{2KN_{\text{MC}}} \sum_{n_{\text{MC}}=1}^{N_{\text{MC}}} \sum_{k=1}^{K} (\theta_k - \hat{\theta}_{k,n_{\text{MC}}})^2 + (\phi_k - \hat{\phi}_{k,n_{\text{MC}}})^2},$$

(60)

is utilized as the evaluation metric, where $(\hat{\theta}_{k,n_{\text{MC}}}, \hat{\phi}_{k,n_{\text{MC}}})$ is the estimate of (θ_k, ϕ_k) for the n_{MC}-th Monte Carlo trial. In addition, the Cramér-Rao bound (CRB) for DOA estimation with coarray processing [53], [54] is presented as reference.

The spatially reshaping approach presents the best estimation accuracy among all tested approaches. Although the CPD of the shifting-embedded coarray tensor $\mathcal{H}$ and the CPD of the spatially reshaped coarray tensor $\mathcal{K}_s$ share a very close accuracy, it has been proved in the *Proposition* that the direct CPD
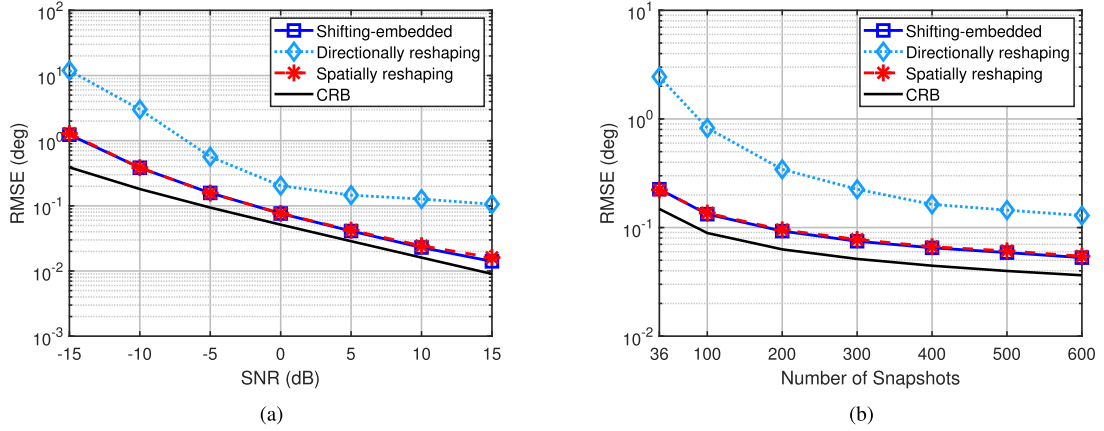
Fig. 5.   Comparison of the estimation accuracy for the proposed algorithm with different coarray tensor structures. (a) RMSE *versus* SNR. (b) RMSE *versus* the number of snapshots.
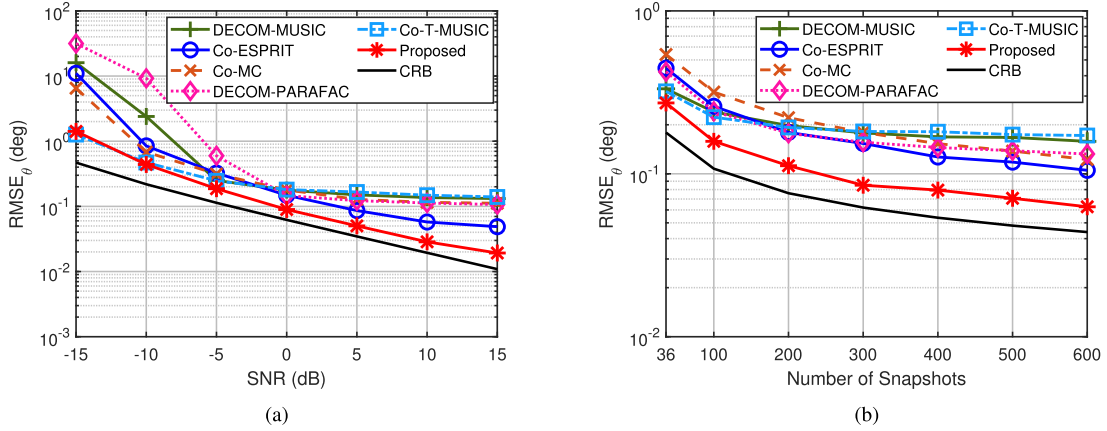

Fig. 6.   Comparison of the azimuth estimation accuracy. (a) RMSE$_\theta$ *versus* SNR. (b) RMSE$_\theta$ *versus* the number of snapshots.

of $\mathcal{H}$ cannot deal with the underdetermined case. Moreover, the directionally reshaping approach has a much worse accuracy compared to the spatially reshaping approach due to the unsatisfactory coarray tensor structure. As such, the optimal coarray tensor structure contributes to an enhanced capability of retrieving angular parameters in both underdetermined and overdetermined cases. In the subsequent simulations, we will only use the spatially reshaped coarray tensor for DOA estimation.

C. Comparison of Estimation Accuracy

In this subsection, we compare the estimation accuracy of the proposed algorithm to those of matrix-based methods including the array decomposition-based MUSIC method ('DECOM-MUSIC') [16], the coarray ESPRIT method ('Co-ESPRIT') [18], and the coarray matrix completion method ('Co-MC') [19], as well as tensor-based methods including the array decomposition-based parallel factor analysis (PARAFAC) method ('DECOM-PARAFAC') [55] and the coarray tensor MUSIC method ('Co-T-MUSIC') [35]. The interval of spectral searching grids for the array decomposition-based methods and the coarray tensor MUSIC method is set to $0.1°$. The RMSEs of

azimuth and elevation estimations

$$\text{RMSE}_\theta = \sqrt{\frac{1}{KN_{\text{MC}}} \sum_{n_{\text{MC}}=1}^{N_{\text{MC}}} \sum_{k=1}^{K} (\theta_k - \hat{\theta}_{k,n_{\text{MC}}})^2},$$

$$\text{RMSE}_\phi = \sqrt{\frac{1}{KN_{\text{MC}}} \sum_{n_{\text{MC}}=1}^{N_{\text{MC}}} \sum_{k=1}^{K} (\phi_k - \hat{\phi}_{k,n_{\text{MC}}})^2}, \qquad (61)$$

are depicted in Figs. 6 and 7, respectively.

It is observed from Figs. 6(a) and 7(a) that the proposed algorithm outperforms the matrix-based methods for the entire simulated regime of SNR. The reason lies in that the proposed algorithm successfully preserves the original structure of multi-dimensional sub-Nyquist signals, whereas the structural information loss brought by the matrix-based model causes performance deterioration. Meanwhile, in comparison to the tensor-based methods, the proposed algorithm shows a further improvement in accuracy, which is benefited from the additionally embedded spatial information in the optimally reshaped coarray tensor. In contrast, the array decomposition-based PARAFAC method implements PARAFAC on the decomposed sparse URA signals, but does not derive augmented coarray tensor statistics.
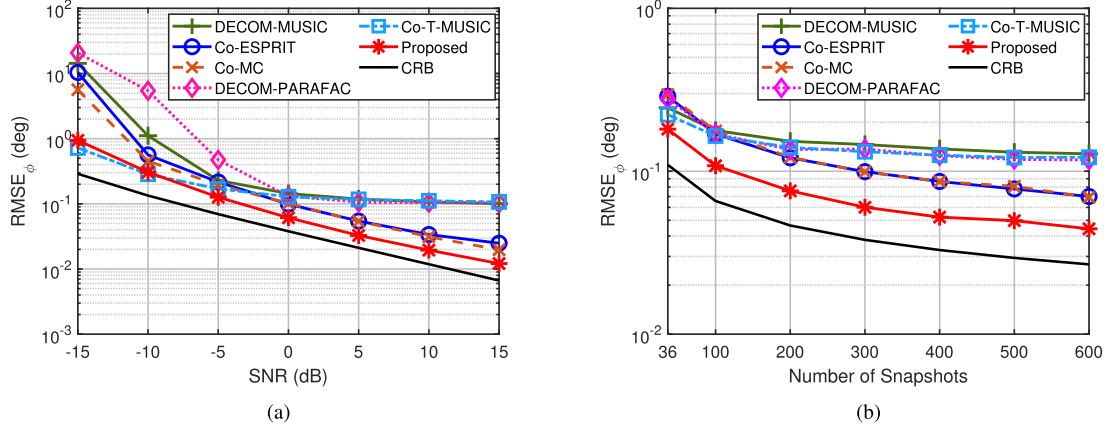
Fig. 7. Comparison of the elevation estimation accuracy. (a) RMSE$_\phi$ *versus* SNR. (b) RMSE$_\phi$ *versus* the number of snapshots.
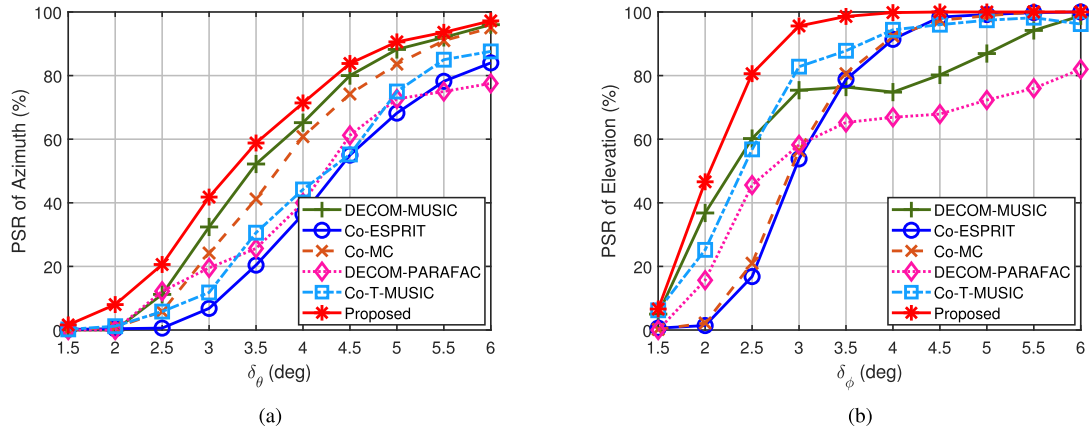

Fig. 8. Comparison of the angular resolution. (a) PSR of azimuth *versus* δ_θ. (b) PSR of elevation *versus* δ_ϕ.

Moreover, the coarray tensor MUSIC method does not consider the optimization of coarray tensor structure, resulting in limited performance as well. Similar simulation results can also be found in Figs. 6(b) and 7(b), where the proposed algorithm exhibits a superior estimation accuracy compared to the other methods for the entire regime of number of snapshots.

D. Comparison of Angular Resolution

The angular resolutions of all tested methods in terms of different azimuth and elevation intervals are compared in Figs. 8(a) and (b), respectively. Two closely spaced sources from directions (θ_1, ϕ_1) and (θ_2, ϕ_2) are considered, where both θ_1 and ϕ_1 are randomly selected within $[20°, 50°]$ following the normal distribution. In Fig. 8(a), θ_2 has an angular spacing of Δ_θ with θ_1 whereas ϕ_2 remains the same as ϕ_1, i.e., $(\theta_2, \phi_2) = (\theta_1 + \delta_\theta, \phi_1)$. In Fig. 8(b), ϕ_2 has an angular spacing of δ_ϕ with ϕ_1 whereas θ_2 remains the same as θ_1, i.e., $(\theta_2, \phi_2) = (\theta_1, \phi_1 + \delta_\phi)$. The evaluated methods are identified to successfully distinguish the two sources if $|\hat{\theta}_{k,n_{MC}} - \theta_k| < \delta_\theta/2$, $|\hat{\phi}_{k,n_{MC}} - \phi_k| < \delta_\theta/2$ in Fig. 8(a), and if $|\hat{\theta}_{k,n_{MC}} - \theta_k| < \delta_\phi/2$, $|\hat{\phi}_{k,n_{MC}} - \phi_k| < \delta_\phi/2$ in Fig. 8(b) for each trial. The probability of successful resolution (PSR) can then be calculated as the percentage of successful trials.

The proposed algorithm presents a greater angular resolution than the matrix-based methods owing to the formulated virtual UCA with an enlarged virtual array aperture, whereas the matrix-based methods cannot formulate multi-dimensional virtual arrays. Moreover, compared to the tensor-based methods, the proposed algorithm manages to augment dimensions of the coarray tensor to enhance the angular resolution. In contrast, the resolution of the array decomposition-based PARAFAC method is limited by physical sparse subarray apertures, and the resolution of the coarray tensor MUSIC method is also unsatisfactory due to the non-ideal coarray tensor structure.

VII. CONCLUSION

In this paper, we proposed a coarray tensor DOA estimation algorithm for structured sparse arrays with an optimal source identifiability. In particular, we derived a coarray tensor from the cross-correlation tensor between sub-Nyquist tensor signals. Then, we revealed that the coarray tensor structure can be properly refined to enhance the source identifiability based on the uniqueness condition for coarray tensor decomposition, which is affected by ranks of the coarray tensor's CP factors. Hence, in order to increase Kruskal's ranks of these CP factors, a dimension increment approach is proposed to flexibly reorganize

coarray tensor statistics and augment the shifting information. The resulting shifting-embedded coarray tensor can then be optimally reshaped to realize the best source identifiability. It is proved that the spatially reshaped coarray tensor offers the maximum number of DOFs, which exceeds the number of physical sensors. As such, the CPD of the spatially reshaped coarray tensor provides closed-form solutions to both azimuth and elevation of sources. Simulation results demonstrate that the proposed algorithm can successfully core with the underdetermined case. Moreover, its performance is superior to those of the competing matrix-based and tensor-based estimation methods in terms of estimation accuracy and angular resolution.

APPENDIX A
SOLUTION OF (49)

The Lagrangian function of (49) can be defined as

$$
\begin{aligned}
\mathcal{L}&(P_x, P_y, \lambda_1, \lambda_2) \\
&= -P_x P_y - (|\mathbb{Q}_x| + 1 - P_x)(|\mathbb{Q}_y| + 1 - P_y) \\
&\quad + \lambda_1(P_x - |\mathbb{Q}_x| + 1) + \lambda_2(P_y - |\mathbb{Q}_y| + 1),
\end{aligned} \tag{62}
$$

where $\{\lambda_1, \lambda_2\}$ are Lagrangian multipliers. The stationary point of (62) exists if and only if the following properties hold,

$$
\text{(i)} \ \frac{\partial \mathcal{L}(P_x, P_y, \lambda_1, \lambda_2)}{\partial P_x} = 0,
$$

$$
\text{(ii)} \ \frac{\partial \mathcal{L}(P_x, P_y, \lambda_1, \lambda_2)}{\partial P_y} = 0,
$$

$$
\text{(iii)} \ \lambda_1(P_x - |\mathbb{Q}_x| + 1) = 0,
$$

$$
\text{(iv)} \ \lambda_2(P_y - |\mathbb{Q}_y| + 1) = 0, \tag{63}
$$

where

$$
\frac{\partial \mathcal{L}(P_x, P_y, \lambda_1, \lambda_2)}{\partial P_x} = -2P_y + (|\mathbb{Q}_y| + 1) + \lambda_1,
$$

$$
\frac{\partial \mathcal{L}(P_x, P_y, \lambda_1, \lambda_2)}{\partial P_y} = -2P_x + (|\mathbb{Q}_x| + 1) + \lambda_2. \tag{64}
$$

Therefore, we have

$$
\begin{aligned}
\lambda_1 &= 2P_y - (|\mathbb{Q}_y| + 1), \\
\lambda_2 &= 2P_x - (|\mathbb{Q}_x| + 1).
\end{aligned} \tag{65}
$$

By respectively substituting the equalities in (65) into Properties (iii) and (iv) in (63), we obtain the solution $P_x = (|\mathbb{Q}_x| + 1)/2$ and $P_y = (|\mathbb{Q}_y| + 1)/2$ as in (50).

APPENDIX B
SOLUTION OF (52)

The Lagrangian function of (52) can be defined as

$$
\begin{aligned}
\mathcal{L}&(P_x, P_y, \lambda_3, \lambda_4, \lambda_5) \\
&= -P_x P_y + \lambda_3(P_x - |\mathbb{Q}_x| + 1) + \lambda_4(P_y - |\mathbb{Q}_y| + 1) \\
&\quad + \lambda_5 \left((|\mathbb{Q}_x| + 1)P_y + (|\mathbb{Q}_y| + 1)P_x - (|\mathbb{Q}_x| + 1)(|\mathbb{Q}_y| + 1)\right),
\end{aligned} \tag{66}
$$

where $\{\lambda_3, \lambda_4, \lambda_5\}$ are Lagrangian multipliers. The stationary point of (66) exists if and only if the following properties hold,

$$
\text{(i)} \ \frac{\partial \mathcal{L}(P_x, P_y, \lambda_3, \lambda_4, \lambda_5)}{\partial P_x} = 0,
$$

$$
\text{(ii)} \ \frac{\partial \mathcal{L}(P_x, P_y, \lambda_3, \lambda_4, \lambda_5)}{\partial P_y} = 0,
$$

$$
\text{(iii)} \ \lambda_3(P_x - |\mathbb{Q}_x| + 1) = 0,
$$

$$
\text{(iv)} \ \lambda_4(P_y - |\mathbb{Q}_y| + 1) = 0,
$$

$$
\text{(v)} \ \lambda_5 \left((|\mathbb{Q}_x| + 1)P_y + (|\mathbb{Q}_y| + 1)P_x \right.
$$
$$
\left. - (|\mathbb{Q}_x| + 1)(|\mathbb{Q}_y| + 1)\right) = 0, \tag{67}
$$

where

$$
\frac{\partial \mathcal{L}(P_x, P_y, \lambda_3, \lambda_4, \lambda_5)}{\partial P_x} = -P_y + \lambda_3 + \lambda_5(|\mathbb{Q}_y| + 1),
$$

$$
\frac{\partial \mathcal{L}(P_x, P_y, \lambda_3, \lambda_4, \lambda_5)}{\partial P_y} = -P_x + \lambda_4 + \lambda_5(|\mathbb{Q}_x| + 1). \tag{68}
$$

Therefore, we have

$$
\begin{aligned}
\lambda_3 &= \lambda_4 = 0, \\
P_y &- \lambda_5(|\mathbb{Q}_y| + 1) = 0, \\
P_x &- \lambda_5(|\mathbb{Q}_x| + 1) = 0,
\end{aligned} \tag{69}
$$

which leads to

$$
\lambda_5 = \frac{P_y}{|\mathbb{Q}_y| + 1} = \frac{P_x}{|\mathbb{Q}_x| + 1} \neq 0. \tag{70}
$$

Then, from Property (v) shown in (67), we know that

$$
(|\mathbb{Q}_x| + 1)P_y + (|\mathbb{Q}_y| + 1)P_x - (|\mathbb{Q}_x| + 1)(|\mathbb{Q}_y| + 1) = 0, \tag{71}
$$

which is equivalent to

$$
P_y = P_x |\mathbb{Q}_y| / (|\mathbb{Q}_x| + 1) + 1. \tag{72}
$$

Substituting (72) into (71) finally leads to $P_x = (|\mathbb{Q}_x| + 1)/2$ and $P_y = (|\mathbb{Q}_y| + 1)/2$.

REFERENCES

[1] H. Zheng, C. Zhou, Y. Gu, and Z. Shi, "Two-dimensional DOA estimation for coprime planar array: A coarray tensor-based solution," in *Proc. IEEE Int. Conf. Acoust., Speech, Signal Process.*, 2020, pp. 4562–4566.

[2] H. L. Van Trees, *Detection, Estimation, and Modulation Theory, Part IV: Optimum Array Processing*. New York, NY, USA: Wiley, 2002.

[3] Z. Zhang, Z. Shi, and Y. Gu, "Ziv-Zakai bound for DOAs estimation," *IEEE Trans. Signal Process.*, vol. 71, pp. 136–149, 2023.

[4] P. P. Vaidyanathan and P. Pal, "Sparse sensing with co-prime samplers and arrays," *IEEE Trans. Signal Process.*, vol. 59, no. 2, pp. 573–586, Feb. 2011.

[5] P. Pal and P. P. Vaidyanathan, "Nested arrays: A novel approach to array processing with enhanced degrees of freedom," *IEEE Trans. Signal Process.*, vol. 58, no. 8, pp. 4167–4181, Aug. 2010.

[6] G. Qin, Y. D. Zhang, and M. G. Amin, "DOA estimation exploiting moving dilated nested arrays," *IEEE Signal Process. Lett.*, vol. 26, no. 3, pp. 490–494, Mar. 2019.

[7] A. Ahmed and Y. D. Zhang, "Generalized non-redundant sparse array designs," *IEEE Trans. Signal Process.*, vol. 69, pp. 4580–4594, 2021.

[8] C. Zhou, Y. Gu, Y. D. Zhang, Z. Shi, T. Jin, and X. Wu, "Compressive sensing-based coprime array direction-of-arrival estimation," *IET Commun.*, vol. 11, no. 11, pp. 1719–1724, Aug. 2017.

[9] G. Qin, M. G. Amin, and Y. D. Zhang, "DOA estimation exploiting sparse array motions," *IEEE Trans. Signal Process.*, vol. 67, no. 11, pp. 3013–3027, Jun. 2019.

[10] X. Wu, "Localization of far-field and near-field signals with mixed sparse approach: A generalized symmetric arrays perspective," *Signal Process.*, vol. 175, Oct. 2020, Art. no. 107665.

[11] J. Li, Y. He, P. Ma, X. Zhang, and Q. Wu, "Direction of arrival estimation using sparse nested arrays with coprime displacement," *IEEE Sensors J.*, vol. 21, no. 4, pp. 5282–5291, Feb. 2021.

[12] J. He, T. Shu, L. Li, and T.-K. Truong, "Mixed near-field and far-field localization and array calibration with partly calibrated arrays," *IEEE Trans. Signal Process.*, vol. 70, pp. 2105–2118, 2022.

[13] P. Pal and P. P. Vaidyanathan, "Coprime sampling and the MUSIC algorithm," in *Proc. IEEE Digit. Signal Process. Signal Process. Educ. Meeting*, 2011, pp. 289–294.

[14] N. Hu, Z. Ye, X. Xu, and M. Bao, "DOA estimation for sparse array via sparse signal reconstruction," *IEEE Trans. Aerosp. Electron. Syst.*, vol. 49, no. 2, pp. 760–773, Apr. 2013.

[15] C. Zhou, Y. Gu, Z. Shi, and M. Haardt, "Structured Nyquist correlation reconstruction for DOA estimation with sparse arrays," *IEEE Trans. Signal Process.*, vol. 71, Mar. 2023.

[16] C. Zhou, Z. Shi, Y. Gu, and X. Shen, "DECOM: DOA estimation with combined MUSIC for coprime array," in *Proc. Int. Conf. Wireless Commun. Signal Process.*, 2013, pp. 1–5.

[17] C.-L. Liu and P. P. Vaidyanathan, "Remarks on the spatial smoothing step in coarray MUSIC," *IEEE Signal Process. Lett.*, vol. 22, no. 9, pp. 1438–1442, Sep. 2015.

[18] C. Zhou and J. Zhou, "Direction-of-arrival estimation with coarray ESPRIT for coprime array," *Sensors*, vol. 17, no. 8, Aug. 2017, Art. no. 1779.

[19] C.-L. Liu, P. P. Vaidyanathan, and P. Pal, "Coprime coarray interpolation for DOA estimation via nuclear norm minimization," in *Proc. IEEE Int. Symp. Circuits Syst.*, 2016, pp. 2639–2642.

[20] S. M. Hosseini and M. A. Sebt, "Array interpolation using covariance matrix completion of minimum-size virtual array," *IEEE Signal Process. Lett.*, vol. 24, no. 7, pp. 1063–1067, Jul. 2017.

[21] C. Zhou, Y. Gu, X. Fan, Z. Shi, G. Mao, and Y. D. Zhang, "Direction-of-arrival estimation for coprime array via virtual array interpolation," *IEEE Trans. Signal Process.*, vol. 66, no. 22, pp. 5956–5971, Nov. 2018.

[22] C. Zhou, Y. Gu, Z. Shi, and Y. D. Zhang, "Off-grid direction-of-arrival estimation using coprime array interpolation," *IEEE Signal Process. Lett.*, vol. 25, no. 11, pp. 1710–1714, Nov. 2018.

[23] Z. Zheng, Y. Huang, W.-Q. Wang, and H. C. So, "Augmented covariance matrix reconstruction for DOA estimation using difference coarray," *IEEE Trans. Signal Process.*, vol. 69, pp. 5345–5358, 2021.

[24] A. J. van der Veen, P. B. Ober, and E. F. Deprettere, "Azimuth and elevation computation in high resolution DOA estimation," *IEEE Trans. Signal Process.*, vol. 40, no. 7, pp. 1828–1832, Jul. 1992.

[25] X. Wu and W.-P. Zhu, "On efficient gridless methods for 2-D DOA estimation with uniform and sparse L-shaped arrays," *Signal Process.*, vol. 191, Feb. 2022, Art. no. 108351.

[26] H. Zheng, C. Zhou, Y. Wang, and Z. Shi, "2-D DOA estimation for coprime cubic array: A cross-correlation tensor perspective," in *Proc. Int. Symp. Antennas Propag.*, 2021, pp. 447–448.

[27] H. Chen, F. Ahmad, S. A. Vorobyov, and F. Porikli, "Tensor decompositions in wireless communications and MIMO radar," *IEEE J. Sel. Topics Signal Process.*, vol. 15, no. 3, pp. 438–453, Apr. 2021.

[28] R. A. Harshman, "Foundations of the PARAFAC procedure: Models and conditions for an explanatory multimodal factor analysis," *UCLA Work. Pap. Phonet.*, vol. 16, p. 84, Dec. 1970.

[29] N. D. Sidiropoulos, R. Bro, and G. B. Giannakis, "Parallel factor analysis in sensor array processing," *IEEE Trans. Signal Process.*, vol. 48, no. 8, pp. 2377–2388, Aug. 2000.

[30] G. Zheng, J. Peng, H. Wang, and Y. Song, "Tensor-based direction of arrival estimation with array virtual translation technique," *IET Signal Process.*, vol. 16, no. 5, pp. 575–587, Jul. 2022.

[31] S. Miron, N. Le Bihan, and J. I. Mars, "Vector-sensor MUSIC for polarized seismic sources localization," *EURASIP J. Adv. Signal Process.*, vol. 2005, Jan. 2005, Art. no. 280527.

[32] I. Podkurkov, G. Seidl, L. Khamidullina, A. Nadeev, and M. Haardt, "Tensor-based near-field localization using massive antenna arrays," *IEEE Trans. Signal Process.*, vol. 69, pp. 5830–5840, 2021.

[33] F. Xu, M. W. Morency, and S. A. Vorobyov, "DOA estimation for transmit beamspace MIMO radar via tensor decomposition with Vandermonde factor matrix," *IEEE Trans. Signal Process.*, vol. 70, pp. 2901–2917, 2022.

[34] H. Zheng, C. Zhou, Z. Shi, and Y. Gu, "Structured tensor reconstruction for coherent DOA estimation," *IEEE Signal Process. Lett.*, vol. 29, pp. 1634–1638, 2022.

[35] K. Han and A. Nehorai, "Nested vector-sensor array processing via tensor modeling," *IEEE Trans. Signal Process.*, vol. 62, no. 10, pp. 2542–2553, May 2014.

[36] L.-T. Huang, A. L. F. de Almeida, and H. C. So, "Target estimation in bistatic MIMO radar via tensor completion," *Signal Process.*, vol. 120, pp. 654–659, Mar. 2016.

[37] L. Liu, J.-F. Gu, and P. Wei, "Joint DOA and frequency estimation with sub-Nyquist sampling," *Signal Process.*, vol. 154, pp. 87–96, Jan. 2019.

[38] S. Na, K. V. Mishra, Y. Liu, Y. C. Eldar, and X. Wang, "TenDSuR: Tensor-based 4D sub-Nyquist radar," *IEEE Signal Process. Lett.*, vol. 26, no. 2, pp. 237–241, Feb. 2019.

[39] H. Zheng, Z. Shi, C. Zhou, M. Haardt, and J. Chen, "Coupled coarray tensor CPD for DOA estimation with coprime L-shaped array," *IEEE Signal Process. Lett.*, vol. 28, pp. 1545–1549, 2021.

[40] J. Shi, F. Wen, and T. Liu, "Nested MIMO radar: Coarrays, tensor modeling, and angle estimation," *IEEE Trans. Aerosp. Electron. Syst.*, vol. 57, no. 1, pp. 573–585, Feb. 2021.

[41] H. Li, W. Cui, C. Jian, H. Xu, and F. Mei, "Two-dimensional DOA estimation for coprime planar arrays based on self-correlation tensor," *Math. Problems Eng.*, vol. 2022, Aug. 2022, Art. no. 7999641.

[42] J. Li, P. Stoica, L. Xu, and W. Roberts, "On parameter identifiability of MIMO radar," *IEEE Signal Process. Lett.*, vol. 14, no. 12, pp. 968–971, Dec. 2007.

[43] X. Guo, D. Brie, S. Zhu, and X. Liao, "A CANDECOMP/PARAFAC perspective on uniqueness of DOA estimation using a vector sensor array," *IEEE Trans. Signal Process.*, vol. 59, no. 7, pp. 3475–3481, Jul. 2011.

[44] H. Zheng, Z. Shi, C. Zhou, and A. L. F. de Almeida, "Coarray tensor completion for DOA estimation," *IEEE Trans. Aerosp. Electron. Syst.*, Mar. 2023.

[45] H. Zheng, C. Zhou, Z. Shi, and A. L. F. de Almeida, "SubTTD: DOA estimation via sub-Nyquist tensor train decomposition," *IEEE Signal Process. Lett.*, vol. 29, pp. 1978–1982, 2022.

[46] A. Weiss, "Blind direction-of-arrival estimation in acoustic vector-sensor arrays via tensor decomposition and Kullback–Leibler divergence covariance fitting," *IEEE Trans. Signal Process.*, vol. 69, pp. 531–545, 2021.

[47] S. Qin, Y. D. Zhang, and M. G. Amin, "Generalized coprime array configurations for direction-of-arrival estimation," *IEEE Trans. Signal Process.*, vol. 63, no. 6, pp. 1377–1390, Mar. 2015.

[48] J. Shi, G. Hu, X. Zhang, F. Sun, and H. Zhou, "Sparsity-based two-dimensional DOA estimation for coprime array: From sum-difference coarray viewpoint," *IEEE Trans. Signal Process.*, vol. 65, no. 21, pp. 5591–5604, Nov. 2017.

[49] Y. Dong, C. Dong, W. Liu, H. Chen, and G. Zhao, "2-D DOA estimation for L-shaped array with array aperture and snapshots extension techniques," *IEEE Signal Process. Lett.*, vol. 24, no. 4, pp. 495–499, Apr. 2017.

[50] N. D. Sidiropoulos and R. Bro, "On the uniqueness of multilinear decomposition of N-way arrays," *J. Chemometrics*, vol. 14, no. 3, pp. 229–239, May 2000.

[51] W. Zheng, X. Zhang, and H. Zhai, "Generalized coprime planar array geometry for 2-D DOA estimation," *IEEE Commun. Lett.*, vol. 21, no. 5, pp. 1075–1078, May 2017.

[52] N. Vervliet, O. Debals, L. Sorber, M. Van Barel, and L. De Lathauwer, "Tensorlab 3.0," Mar. 2016. [Online]. Available: http://www.tensorlab.net

[53] C.-L. Liu and P. P. Vaidyanathan, "Cramér–Rao bounds for coprime and other sparse arrays, which find more sources than sensors," *Digit. Signal Process.*, vol. 61, pp. 43–61, Feb. 2017.

[54] M. Wang and A. Nehorai, "Coarrays, MUSIC, and the Cramér-Rao bound," *IEEE Trans. Signal Process.*, vol. 65, no. 4, pp. 933–946, Feb. 2017.

[55] X. Wang, M. Huang, and L. Wan, "Joint 2D-DOD and 2D-DOA estimation for coprime EMVS-MIMO radar," *Circuits, Syst. Signal Process.*, vol. 40, pp. 2950–2966, Jan. 2021.

Hang Zheng (Graduate Student Member, IEEE) received the B.E. degree in transportation engineering from Tongji University, Shanghai, China, in 2019. He is currently working toward the Ph.D. degree with the College of Information Science and Electronic Engineering, Zhejiang University, Hangzhou, China. He is also a Visiting Student with Aalto University, Espoo, Finland. His research interests include array signal processing, tensor signal processing, and machine learning. He was the recipient of the Best Paper Award from ISAP 2020 and ICAUS 2022.

Chengwei Zhou (Member, IEEE) received the Ph.D. degree in electronic science and technology from Zhejiang University, Hangzhou, China, in 2018. He was a Visiting Researcher with the University of Technology Sydney, Sydney, NSW, Australia, from April 2017 to October 2017. He was a Postdoctoral Research Fellow with the State Key Laboratory of Industrial Control Technology, the College of Control Science and Engineering, Zhejiang University, Hangzhou, China, from 2018 to 2020. Since June 2020, he has been a Research Associate Professor with the College of Information Science and Electronic Engineering, Zhejiang University. His research interests include array signal processing, direction-of-arrival estimation, and adaptive beamforming. Dr. Zhou is currently an Associate Editor for *International Journal of Communication Systems*, and an Editorial Board Member of *Journal of Signal Processing* (in Chinese). He was the recipient of the 2021 IEEE Signal Processing Society Young Author Best Paper Award, ISAP 2020 Best Paper Award, and 2019 IET Communications Premium Award.

Yujie Gu (Senior Member, IEEE) received the Ph.D. degree in electronic engineering from Zhejiang University, Hangzhou, China, in 2008. After graduation, he held multiple research positions in China, Canada, Israel, and the USA. He is currently a Senior Radar Scientist with Aptiv working on research and development of advanced automotive radar system. His research interests include statistical and array signal processing including robust adaptive beamforming, information theoretic sensing, spatial spectrum estimation, and performance bound analysis. Dr. Gu is the Subject Editor-in-Chief of *Electronics Letters* and an Associate Editor for *Signal Processing*. He was the Lead Guest Editor of the special issue on Source Localization in Massive MIMO for Digital Signal Processing. He was the Special Sessions Co-Chair of the 2020 IEEE Sensor Array and Multichannel Signal Processing Workshop. He is an Elected Member of the Sensor Array and Multichannel (SAM) Technical Committee and the Signal Processing Theory and Methods (SPTM) Technical Committee of the IEEE Signal Processing Society. He was the recipient of the 2019 IET Communications Premium Award, and coauthored a paper that was the recipient of the 2021 IEEE Signal Processing Society Young Author Best Paper Award.

Zhiguo Shi (Senior Member, IEEE) received the B.S. and Ph.D. degrees in electronic engineering from Zhejiang University, Hangzhou, China, in 2001 and 2006, respectively. Since 2006, he has been a Faculty Member with the College of Information Science and Electronic Engineering, Zhejiang University, where he is currently a Full Professor. From 2011 to 2013, he visited the Broadband Communications Research Group, University of Waterloo, Waterloo, ON, Canada. His research interests include array signal processing, localization, and Internet-of-Things. Prof. Shi was the recipient of the 2019 IET Communications Premium Award, and coauthored a paper that was the recipient of the 2021 IEEE Signal Processing Society Young Author Best Paper Award. He was also the recipient of the Best Paper Award from ISAP 2020, IEEE GLOBECOM 2019, IEEE WCNC 2017, IEEE/CIC ICCC 2013, and IEEE WCNC 2013. He was the General Co-Chair of IEEE SAM 2020 and was the Editor of the IEEE NETWORK. He is currently an Associate Editor for the IEEE SIGNAL PROCESSING LETTERS, IEEE TRANSACTIONS ON VEHICULAR TECHNOLOGY, *IET Communications*, and *Journal of the Franklin Institute*. He is an elected member of the Sensor Array and Multichannel (SAM) Technical Committee of the IEEE Signal Processing Society.

Yimin D. Zhang (Fellow, IEEE) received the Ph.D. degree from the University of Tsukuba, Tsukuba, Japan, in 1988. He is currently an Associate Professor with the Department of Electrical and Computer Engineering, Temple University, Philadelphia, PA, USA. From 1998 to 2015, he was a Research Faculty with the Center for Advanced Communications, Villanova University, Villanova, PA, USA. His research interests include array signal processing, compressive sensing, machine learning, convex optimization, and time-frequency analysis with applications to radar, wireless communications, and satellite navigation. Dr. Zhang is the Senior Area Editor of IEEE TRANSACTIONS ON SIGNAL PROCESSING and an Associate Editor for *Signal Processing*. He was an Associate Editor for IEEE TRANSACTIONS ON SIGNAL PROCESSING, IEEE TRANSACTIONS ON AEROSPACE AND ELECTRONIC SYSTEMS, IEEE SIGNAL PROCESSING LETTERS, and *Journal of the Franklin Institute*. He was the Technical Co-Chair of the 2018 IEEE Sensor Array and Multichannel Signal Processing Workshop. He was the recipient of the 2016 IET Radar, Sonar Navigation Premium Award, the 2017 IEEE Aerospace and Electronic Systems Society Harry Rowe Mimno Award, the 2019 IET Communications Premium Award, and the 2021 EURASIP Best Paper Award for Signal Processing. He coauthored two papers that respectively received the 2018 and 2021 IEEE Signal Processing Society Young Author Best Paper Awards. He is a Fellow of SPIE.